Precambrian Research 164 (2008) 16–39

Contents lists available at ScienceDirect

Precambrian Research

journal homepage: www.elsevier.com/locate/precamres

Zircon geochronology and Sr, Nd, Pb isotope geochemistry of granitoids from Bayuda Desert and Sabaloka (Sudan): Evidence for a Bayudian event (920–900 Ma) preceding the Pan-African orogenic cycle (860–590 Ma) at the eastern boundary of the Saharan Metacraton

Dirk Küster[a,d,*], Jean-Paul Liégeois[a,**], Dmitry Matukov[b], Sergei Sergeev[b], Friedrich Lucassen[c]

[a] Royal Museum for Central Africa, Isotope Geology Section, B-3080 Tervuren, Belgium
[b] Center for Isotopic Research, All-Russian Geological Research Institute (VSEGEI), 74 Sredny Prospect, RU-199106 St.-Petersburg, Russia
[c] GeoForschungsZentrum Potsdam, Telegrafenberg, D-14473 Potsdam, Germany
[d] Technische Universität Berlin, Institut für Angewandte Geowissenschaften, FG Mineralogie-Petrologie, Ackerstr. 71-76, D-13355 Berlin, Germany

ARTICLE INFO

Article history:
Received 13 July 2007
Received in revised form 8 February 2008
Accepted 10 March 2008

Keywords:
Saharan Metacraton
Granitoids
Zircon geochronology
Neoproterozoic
Pan-African
Bayudian

ABSTRACT

Results of zircon geochronology and Sr, Nd and Pb isotope investigations carried out on granitoid rocks from the boundary of the Saharan Metacraton with the Arabian–Nubian Shield (ANS) reveal a protracted, partly pre-Pan-African geodynamic evolution and the existence of crustal terranes of different ancestries. (Meta)granitoids and gneisses in north-central Bayuda Desert record a 920–900 Ma orogenic event, hitherto unrecognized in northeastern Africa. This early Neoproterozoic Bayudian event is restricted to a pre-Pan-African crustal terrane which appears only slightly affected by Pan-African tectogenesis and deformation, named here the Rahaba–Absol terrane. Within this terrane, amphibolite-facies metamorphism occurred at 921 ± 10 Ma in the El Melagi muscovite–biotite gneiss of the Rahaba Series, probably during a collisional phase; followed by the intrusion of the Absol medium-K granite–granodiorite pluton discordantly emplaced at 900 ± 9 Ma into high-grade schists and amphibolites of the metavolcanosedimentary Absol Series. Nd T_{DM} model ages (2040–2430 Ma) and ages of rounded zircon cores (1060, 1980, 2540 and 2675 Ma) of the El Melagi gneiss indicate a predominantly late Archaean to Palaeoproterozoic source region and suggest a latest Mesoproterozoic to early Neoproterozoic depositional age of its pelitic precursor sediment. The post-collisional Absol pluton has isotope characteristics ($\varepsilon_{Nd\ 900}$ of −0.3 to −4.3, T_{DM} model ages: 1300–1830 Ma, $SrIR_{900}$ of 0.7028–0.7055, $^{207}Pb/^{204}Pb$ of 15.66–15.81) indicating assimilation of old pre-Neoproterozoic crust. The Rahaba–Absol terrane is part of the Saharan Metacraton and is in tectonic contact with the high-grade metamorphic Kurmut terrane of eastern Bayuda Desert. The Kurmut terrane has juvenile Neoproterozoic isotope characteristics, its granitoids record only Pan-African orogenic events and it is therefore considered a part of the Arabian–Nubian Shield. Within the Kurmut terrane the Dam Et Tor medium-K epidote–biotite gneiss gave a concordant zircon age of 858 ± 9 Ma, interpreted as the crystallization age of the volcanic/subvolcanic precursor of the gneiss. Isotopic data of the Dam Et Tor gneiss ($\varepsilon_{Nd\ 858}$ of 5.7–6.1, T_{DM} model ages: 860–900 Ma, $SrIR_{858}$ of 0.7026–0.7028, $^{207}Pb/^{204}Pb$ of 15.46) indicate a depleted mantle source and an oceanic arc magmatic environment. The age of the amphibolite-facies metamorphism and deformation of the Dam Et Tor gneiss and its enclosing metavolcanosedimentary Kurmut Series is best approached by a Sm–Nd isochron age (806 ± 19 Ma; Küster and Liégeois [Küster, D., Liégeois, J.P., 2001. Sr, Nd isotopes and geochemistry of the Bayuda Desert high-grade metamorphic basement (Sudan): an early Pan-African oceanic convergent margin, not the edge of the East Saharan ghost craton? Prec. Res., 109, 1–23]). Both the Rahaba–Absol and the Kurmut terrane of the Bayuda Desert are intruded by post-collisional high-K granitoid magmatism of late Pan-African age, with no intermediate events recorded. The An Ithnein pluton that intrudes the pre-Pan-African Rahaba–Absol terrane is dated at 597 ± 4 Ma. The isotope characteristics of this pluton ($\varepsilon_{Nd\ 600}$ of −1.5 to 2.4, T_{DM} model ages: 910–1190 Ma, $SrIR_{600}$ of 0.7011–0.7038, $^{207}Pb/^{204}Pb$ of 15.59–15.69) and that of the Nabati pluton intruding the Kurmut terrane ($\varepsilon_{Nd\ 600}$ of 0.1–4.5, T_{DM} model ages: 750–1050 Ma, $SrIR_{600}$ of 0.7032–0.7036,

* Corresponding author at: Technische Universität Berlin, Institut für Angewandte Geowissenschaften, FG Mineralogie-Petrologie, Ackerstr. 71-76, D-13355 Berlin, Germany. Tel.: +49 30 314 72084; fax: +49 30 314 72218.
** Corresponding author. Fax: +32 2 650 2252.
E-mail addresses: kuesterreeck@yahoo.de (D. Küster), jean-paul.liegeois@africamuseum.be (J.-P. Liégeois).

0301-9268/$ – see front matter
doi:10.1016/j.precamres.2008.03.003

$^{207}Pb/^{204}Pb$ of 15.56–15.60) indicate a derivation from a juvenile crustal source or the mantle with limited assimilation of older crust. Post-collisional late Pan-African granite plutons at Sabaloka, south of Bayuda Desert, are distinguished into high-K and shoshonitic suites. The Banjedid high-K pluton was emplaced at 605 ± 4 Ma, while the Babados shoshonitic pluton intruded at 591 ± 5 Ma. Magmatic zircons from both plutons have rims with low Th/U ratios, suggesting a HT metamorphic event contemporaneous with magma emplacement. Both granitoid suites have isotopic characteristics ($\varepsilon_{Nd\ 600}$ of −8.3 to −2.1, T_{DM} model ages: 1160–1560 Ma, $SrIR_{600}$ of 0.7029–0.7069, $^{207}Pb/^{204}Pb$ of 15.72–15.81) indicating the assimilation of older pre-Neoproterozoic crust. Sabaloka is thus clearly identified as a part of the Saharan Metacraton but is distinguished from the Rahaba–Absol terrane by a strong Pan-African high-grade metamorphic imprint [Kröner, A., Stern, R.J., Dawoud, A.S., Compston, W., Reischmann, T., 1987. The Pan-African continental margin in northeastern Africa: evidence from a geochronological study of granulites at Sabaloka, Sudan. Earth Planet. Sci. Lett. 85, 91–104] indicating the likely existence of a discrete Sabaloka terrane.

1. Introduction

The Precambrian basement in the central and eastern Sahara dominantly consists of high-grade gneisses, migmatites and supracrustal rocks. Geochronological and isotopic data show that this continental crust is heterogeneous, containing both pre-Neoproterozoic rocks with intense Neoproterozoic remobilisation as well as juvenile Neoproterozoic crustal materials (Küster and Liégeois, 2001; Abdelsalam et al., 2002; and references therein). The basement is referred to as the Saharan Metacraton (Abdelsalam et al., 2002), emphasizing that during the Neoproterozoic Pan-African orogenic cycle it neither behaved as a stable craton nor as a classical mobile belt. Instead, Neoproterozoic events are characterized by metamorphism, granitoid magmatism and deformation. Following Abdelsalam et al. (2002) several processes – or a combination of these – have been advocated to explain the Neoproterozoic remobilisation of the Saharan Metacraton: (1) collision; (2) delamination of the subcontinental lithospheric mantle; (3) extension; and (4) assembly of the metacraton from exotic terranes. The geodynamical history of the Saharan Metacraton is however still poorly known.

The Saharan Metacraton stretches between the Tuareg Shield in the west, the Arabian–Nubian Shield (ANS) in the east and the Congo Craton in the south (Fig. 1). Its borders have been defined based on lithological, tectonic and geochronological evidences. To the north, rocks of the metacraton disappear beneath the Phanerozoic cover of the northern margin of Africa. The eastern boundary of the Saharan Metacraton against the ANS is tectono-lithological in nature, it is marked by the Keraf-Kabus-Sekerr Suture (see Fig. 1) along which high-grade metamorphic rocks of the Saharan Metacraton are juxtaposed against low-grade metavolcanosedimentary juvenile Neoproterozoic rocks of the ANS. The Keraf-Kabus-Sekerr Suture has been interpreted as an arc-continental suture (Abdelsalam and Stern, 1996). However, in its northern part Küster and Liégeois (2001) have found Neoproterozoic high-grade rocks west of the Keraf Suture indicating that the boundary between the ANS and the Saharan Metacraton may lie further west or that these high-grade Neoproterozoic rocks have been thrust across the metacraton.

In order to get more precise information of the geodynamical evolution along the northern part of the ANS/Saharan Metacraton boundary we have studied granitoid rocks at Bayuda Desert and Sabaloka in north-central Sudan (Figs. 1–3). The study area in Bayuda Desert has a size of ~25,000 km^2, while basement rocks at Sabaloka are exposed over an area of ~5000 km^2; together both regions cover an area almost equal in size to Belgium. Both the Bayuda Desert and Sabaloka lie immediately west of the Keraf Suture and hence are considered constituents of the Saharan Metacraton. In the paper we use geochemical, geochronological, and isotopic data of granitoid orthogneisses and of post-collisional granite plutons to identify the settings, ages and sources of dif-

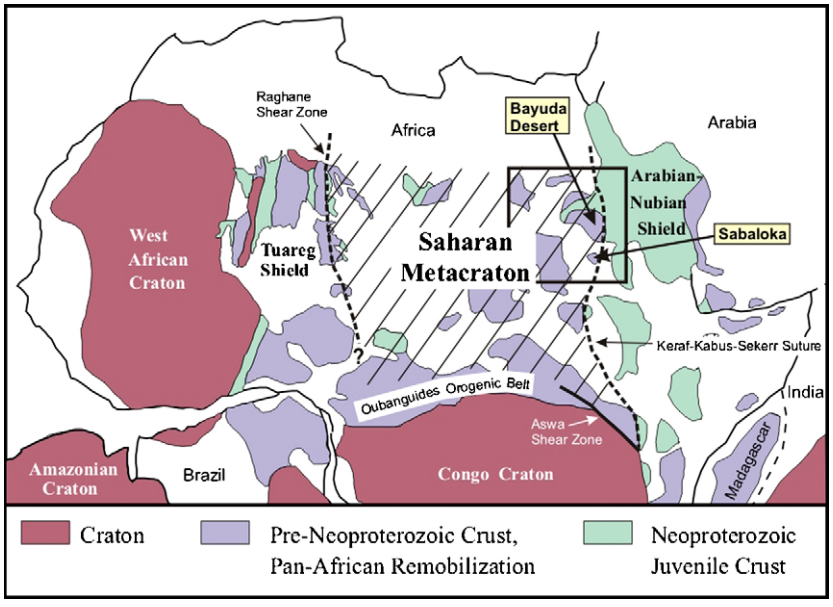

Fig. 1. Geological sketch map of the Saharan Metacraton.

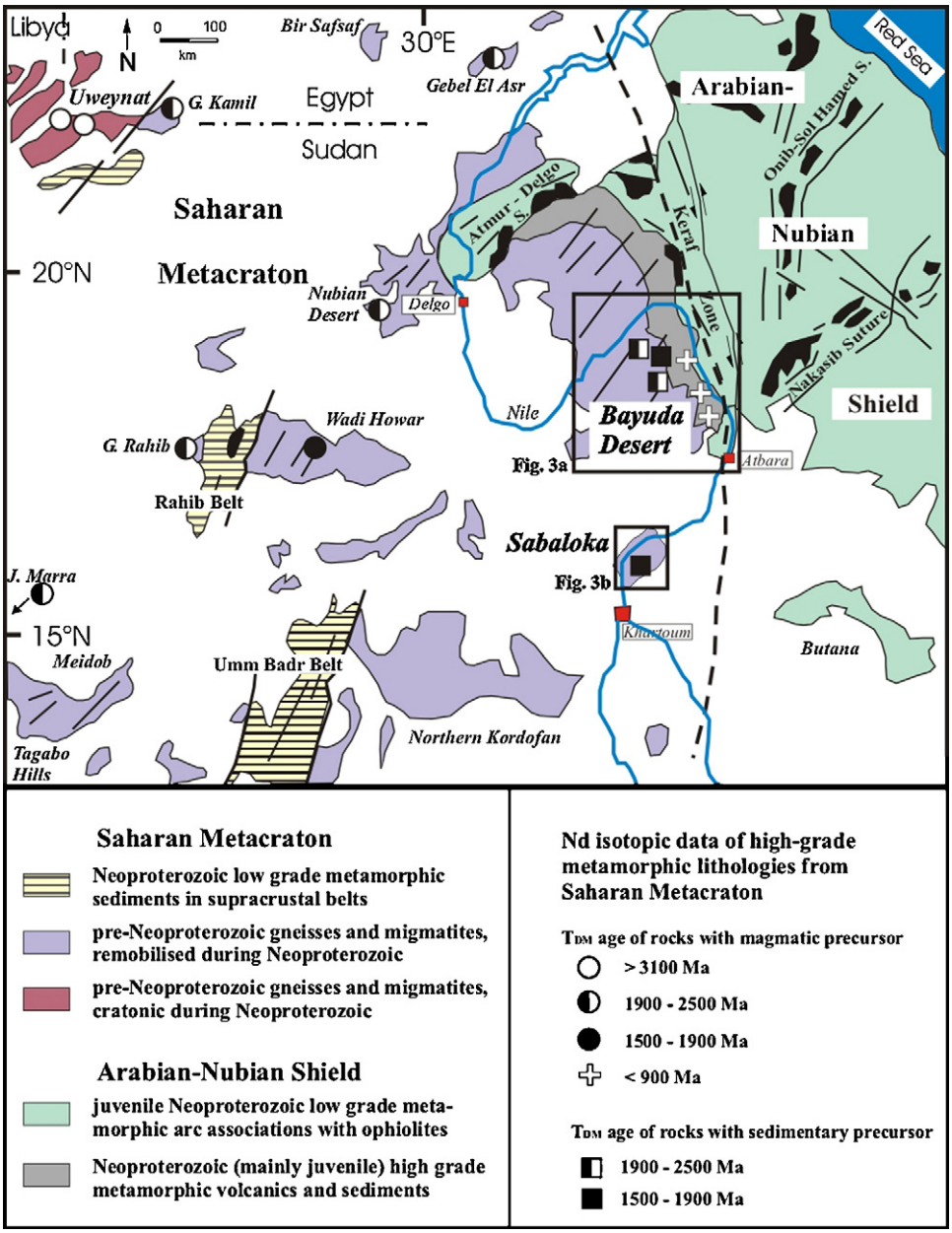

Fig. 2. Geological sketch map of northeastern part of the Saharan Metacraton with major lithostructural units. Nd isotopic data are from Klerkx and Deutsch (1977), Harris et al. (1984), Kröner et al. (1987), Harms et al. (1990), Küster and Liégeois (2001).

ferent episodes of granitoid magmatism and to gain more insight into the history, composition and structure of the continental crust along the eastern edge of the Saharan Metacraton. In doing so we refer to the term Pan-African in the sense of a protracted orogenic cycle (or even cycles) which lasted from ca. 850 Ma to c.550 Ma and which included several distinguished magmatic and tectonic events. Knowing that the time span of ~300 million years is much too long for an individual orogeny we have nonetheless retained this use of Pan-African since it has become a common practice in scientific literature during the past 25 years. We note here however the urgent need for a more focused definition of Pan-African (cf. Stern, 2008), an issue which is beyond the scope of this paper. For reasons of convenience we have therefore distinguished in our study (1) an early Pan-African accretionary phase (~850 to 650 Ma) which mainly consists of subductional magmatism and accretion of oceanic terranes and (2) the main Pan-African phase (~650 to 550 Ma) which corresponds to collisional and post-collisional processes during Gondwana formation. The abundant post-collisional granitoids (600–550 Ma) are considered as late Pan-African. The latter phase is a mainly intracontinental event in NE-Africa, even if large movements occurred along mega-shear zones.

2. Structural and geochronological framework of the north-eastern part of the Saharan Metacraton

Rocks of the Saharan Metacraton are patchily exposed in northwestern, central and western Sudan and in south-western Egypt (Fig. 2). They are predominantly made up of high-grade metamorphic gneisses, migmatites and supracrustal rocks, commonly foliated along ENE–WSW to NE–SW structures. This structural trend has been named the Zalingei folded zone (Vail, 1976) and

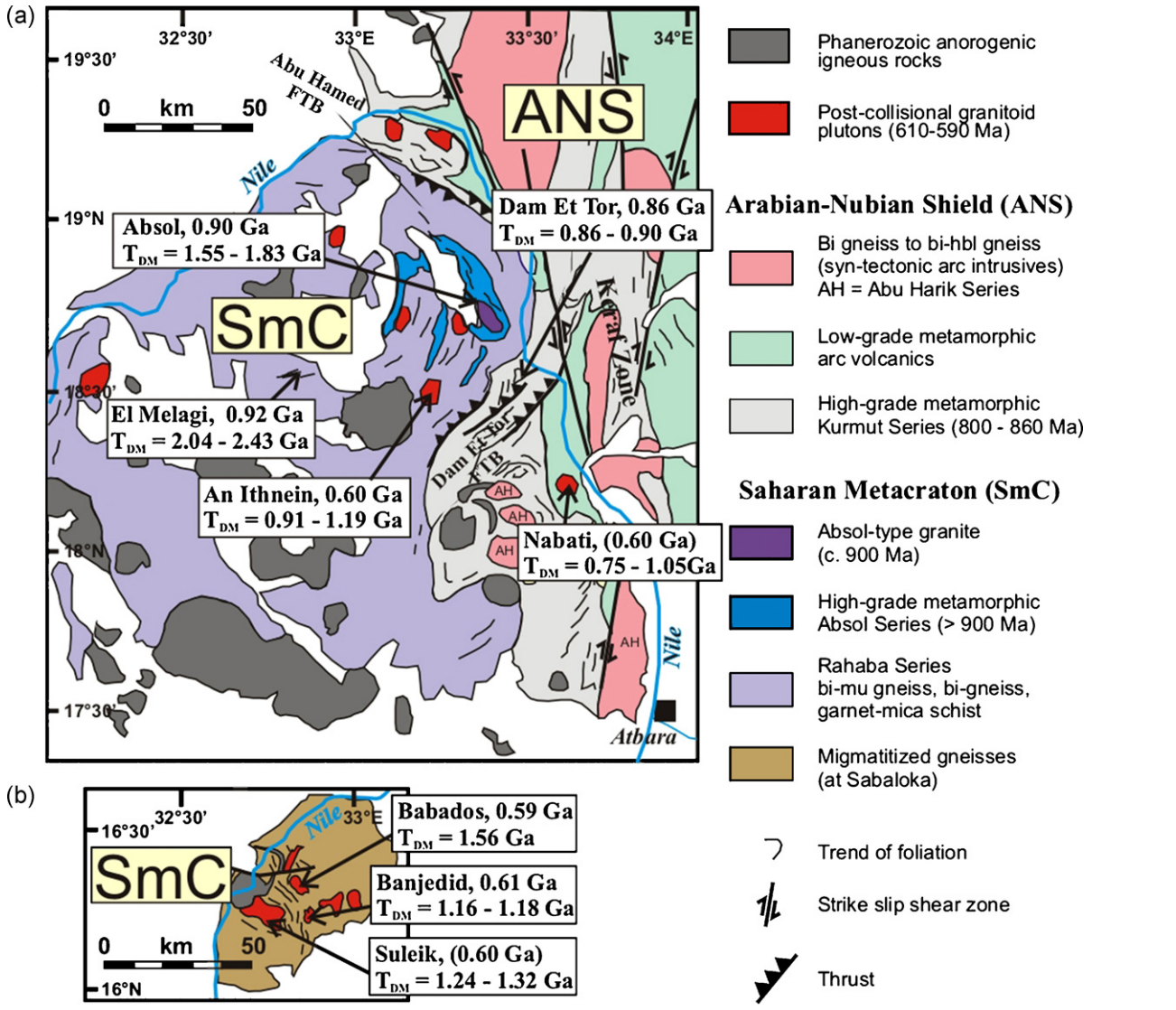

Fig. 3. Geological sketch map of (a) Bayuda Desert, and (b) Sabaloka with location of investigated granitoids. Also shown are their U–Pb zircon ages and Nd T_{DM} model ages, all determined in this study. The maps have been compiled from Barth and Meinhold (1979), Kröner et al. (1987), Abdelsalam et al. (1998), Bailo et al. (2003) and have been modified according to the findings of this investigation. See text for further explanation.

an early Neoproterozoic or even pre-Neoproterozoic age has been assigned to it (Vail, 1989). Overlying the high-grade rocks are supracrustal belts, namely the Rahib and Umm Badr Belts (Fig. 2), which consist of low-grade metamorphic sedimentary and volcanic rocks of rift-type origin (Schandelmeier et al., 1990). These belts strike NNE–SSW, oblique to the older NE–SW structures, and are most probably Neoproterozoic in age (Schandelmeier et al., 1990).

Nd isotopic data of the high-grade basement of the north-eastern Saharan Metacraton suggest Archaean, Palaeoproterozoic and Neoproterozoic ancestries with a direction of approximate crustal growth from NW to SE. Archaean crust (Nd T_{DM} ages > 3100 Ma, Harris et al., 1984) is exposed only in the Uweynat massif of SE Libya/SW Egypt (Fig. 2). The Uweynat crust was not remobilised during the Neoproterozoic (Rb–Sr isochron ages of 2673 ± 21 Ma from charnockitic gneisses and of 1836 ± 43 Ma from migmatites, Klerkx and Deutsch, 1977). Uweynat could constitute a cratonic fragment within the Saharan Metacraton; however it has been intruded by Cenozoic alkaline ring-complexes (André et al., 1991; Conticelli et al., 1995) suggesting rather that it is a well-preserved part of the metacraton but not anymore truly cratonic.

In SW Egypt (Gebel Kamil, Gebel El Asr), NW Sudan (Nubian Desert, Gebel Rahib) and W Sudan (Gebel Marra region) isotopic data of tonalitic and granitic orthogneisses and of migmatites have confirmed the existence of mainly Palaeoproterozoic crust (Nd T_{DM} ages between 1900 and 2500 Ma, Harris et al., 1984; Harms et al., 1990); slightly younger Nd T_{DM} ages of 1600–1700 Ma (Harms et al., 1990) were found in tonalitic gneisses at Wadi Howar (Fig. 2). This Palaeoproterozoic basement was intensely remobilised and deformed during the Neoproterozoic Pan-African orogeny (Harms et al., 1990; Schandelmeier et al., 1990).

In Bayuda Desert and at Sabaloka, close to the ANS/Saharan Metacraton boundary (Fig. 2) medium- to high-grade metasedimentary schists and gneisses have Nd T_{DM} ages between 1600 and 2400 Ma (Harris et al., 1984; Kröner et al., 1987; Küster and Liégeois, 2001). At Sabaloka, these metasedimentary garnet–cordierite–gneisses contain detrital zircons ranging in age from 900 to 2600 Ma and indicate an early Neoproterozoic depositional age (Kröner et al., 1987). In eastern Bayuda Desert, immediately to the west of the ANS, high-grade metavolcano-sedimentary gneisses and amphibolites have Nd T_{DM} ages in the

range 900–790 Ma and represent an early Pan-African island arc association dated at ca. 800 Ma by the Sm–Nd method (Küster and Liégeois, 2001).

Post-collisional late Pan-African (600–560 Ma) granites are abundant in the entire north-eastern Saharan Metacraton, with exception of the Uweynat massif. This granitoid magmatism is contemporaneous with an escape tectonics along major strike-slip shear zones, uplift and extension of the entire Pan-African orogen in northeastern Africa (cf. Stern, 1994; Küster and Harms, 1998).

3. Outline of geology and structures along the eastern boundary of the Saharan Metacraton

The N–S trending Keraf Suture Zone is one of the late Neoproterozoic shear zones that acts as the ~500 km long and ~50 km wide divide between the north-eastern Saharan Metacraton and the Arabian–Nubian Shield (Figs. 2 and 3). Transpressive deformation along the Keraf Zone was multiphase and lasted from ~650 to ~570 Ma (Abdelsalam et al., 1998). It was caused by NW–SE oblique convergence between the ANS and the Saharan Metacraton and produced N-trending upright folds in the northern Keraf Zone (Fig. 2) and N- and NNW-trending, sinistral, strike-slip faults in the southern Keraf Zone (Abdelsalam et al., 1998). The N–S trending Keraf trend truncates older NE–SW structures of the Saharan Metacraton (Zalingei trend) and also of the ANS (Fig. 2). In the central ANS, NE–SW oriented structures include ophiolite decorated suture zones, e.g. the Nakasib Suture (cf. Schandelmeier et al., 1994b) or the Onib-Sol Hamed Suture (Fig. 2). These suture zones mark boundaries and collision zones between individual island arc terranes. Arc collisions and suturing in the ANS was largely completed by 760–700 Ma (Abdelsalam and Stern, 1996; Schandelmeier et al., 1994b). Another NE–SW trending ophiolite decorated suture is the Atmur-Delgo Suture (cf. Schandelmeier et al., 1994a) in the Nubian Desert (Fig. 2). Along this suture, subduction-derived low-grade rocks of ANS derivation were thrust southeastwards onto the high-grade basement of the Saharan Metacraton (Schandelmeier et al., 1994a; Harms et al., 1994; Abdelsalam et al., 1995, 1998). Deformation and nappe emplacement along the Atmur-Delgo Suture were completed before 700 Ma ago (Abdelsalam et al., 1995).

In the Bayuda Desert, pre-Keraf structures can be seen in the form of rock foliations but also in two fold and thrust belts: (1) the NE–SW striking Dam Et Tor Fold/Thrust Belt in the east-central Bayuda Desert and (2) the NW–SE-striking Abu Hamed Fold/Thrust Belt in the northern Bayuda Desert (Abdelsalam et al., 1998; Fig. 3). Along the Dam Et Tor Thrust Belt high-grade supracrustal rocks (kyanite and garnet schists) are thrust to the SE over rocks of relatively lower metamorphic grade (Abdelsalam et al., 1998). Along the Abu Hamed Thrust Belt biotite gneisses are thrust to the NE over micaschists and garnet–staurolite schists (Abdelsalam et al., 1998). Both thrusts are partially decorated by talc–carbonate schists. Furthermore, in the north-eastern Bayuda Desert, foliations change from E–W to NW–SE in the Abu Hamed Belt to NNW–SSE and almost N–S along the Nile and finally to NE–SW in the Dam Et Tor Belt; consequently, both fold and thrust belts might be connected to form one common arc-like fold and thrust belt (Fig. 3).

The geodynamical significance of these >650 Ma pre-Keraf deformations in the northeastern Saharan Metacraton (Bayuda Desert/Sabaloka), but also in neighbouring parts of the ANS is not resolved. Abdelsalam et al. (1995) call this the Atmur deformation and link it with NW–SE directed oblique convergence between terranes of both Saharan Metacraton and ANS derivation. The age of this collisional deformation is likely to be older than 715 Ma, which is the age of undeformed post-tectonic granite plutons in the Keraf Zone (Fig. 2; Bailo et al., 2003), or even 760 Ma if the granites of the Nakasib Belt in the ANS are considered (Fig. 2; Schandelmeier et al., 1994b). In the Keraf Suture, Bailo et al. (2003) have also investigated juvenile Neoproterozoic granitoid orthogneisses (Nd T_{DM} ages < 900 Ma) and dated them with zircon evaporation technique at 735 Ma. This age is interpreted as either the age of the magmatic protolith or the age of metamorphism and deformation of the orthogneiss (Bailo et al., 2003). In the Saharan Metacraton, granitoid plutonism related to the 700–750 Ma time span has not been dated. However, muscovite cooling ages in Bayuda Desert indicate terminal cooling of this tectonometamorphic phase at ~670 Ma (Küster, 1995). Furthermore, at Sabaloka, Kröner et al. (1987) dated granulite facies metamorphism at approximately 700–720 Ma, followed by a retrograde migmatisation under amphibolite-facies conditions at ca. 570 Ma. While the older metamorphism probably dates the collisional event(s) along the eastern boundary of the Saharan Metacraton, the younger retrogression is coeval with uplift and post-collisional granitoid magmatism in the region (cf. Küster and Harms, 1998). In the Bayuda Desert, two post-collisional granite plutons were dated with Rb–Sr whole rock technique and gave ages of 573 Ma (Meinhold, 1979) and 549 Ma (Ries et al., 1985). Post-collisional granites have not been dated at Sabaloka.

3.1. Subdivision of the Bayuda Desert basement

The Bayuda Desert is characterized by high-grade metamorphic rocks, distinct form the low-grade metamorphic arc volcanics of the ANS located to the east of River Nile (Figs. 2 and 3). Historically, this high-grade Bayuda Desert basement has been separated in two main zones (Vail, 1971, 1988): a Grey Gneiss Unit mainly made up of monotonous grey granitoid gneisses in western and central Bayuda Desert (Rahaba Series in Fig. 3) and a Metasedimentary Unit composed of felsic gneisses, amphibolites, various schists, quartzites and calc-silicate rocks in eastern Bayuda Desert (Kurmut and Absol Series in Fig. 3). Based on their regional mapping Barth and Meinhold (1979) and Meinhold (1979) have further subdivided Vail's Metasedimentary Unit into the Kurmut and Absol Series and called the Grey Gneiss Unit the Rahaba Series. They grouped these three Series within a Bayuda Formation. In the southeastern most part of Bayuda Desert they also outlined the Abu Harik Series, made up of biotite and biotite–hornblende gneisses and considered as a remnant of an old basement (Meinhold, 1979).

The Kurmut Series occupies the eastern part of Bayuda Desert south of the Dam Et Tor Fold/Thrust Belt, and reoccurs north of the Abu Hamed Fold/Thrust Belt in the northernmost Bayuda Desert (Fig. 3; Barth and Meinhold, 1979; Meinhold, 1979). It is made up of (in order of importance) biotite and biotite–hornblende gneisses, amphibolites and hornblende gneisses, quartzites and quartzitic schists, various mica schists, calc-silicates and marbles. The grade of metamorphism is that of low to medium amphibolite facies (Meinhold, 1979). The Absol Series is found in the northeastern part of the Bayuda Desert (south of the Abu Hamed Thrust Belt and north of the Dam Et Tor Thrust Belt; Fig. 3), and is composed of (in order of importance) various mica schists (quartz–mica schist, kyanite–staurolite–garnet–mica schist, tourmaline mica schist, graphitic and manganiferous schist, ferruginous quartzite), amphibolites and hornblende gneisses. The Absol Series interfingers with the gneissic quartzo-feldspathic Rahaba Series and, in such cases, always forms the cores of synclinal structures (Barth and Meinhold, 1979). According to these authors the Rahaba Series also subordinately contains garnetiferous mica schists and rare amphibolites. Both Series record metamorphism under upper amphibolite-facies conditions up to incipient migmatisation (Meinhold, 1979). In the field, there is thus a clear association between the Absol and Rahaba Series while the Kurmut Series appears to be in tectonic contact with the two former Series.

4. Sampling and analytical techniques

We have sampled deformed granitoid orthogneisses as well as undeformed granitoid plutons in Bayuda Desert and at Sabaloka and subjected them to geochemical, isotope geochemical and geochronological investigations. Sampled occurrences are indicated on the geological sketch map of Fig. 3.

Major elements were determined by X-ray fluorescence (XRF) at Technische Universität Berlin. Trace elements were analyzed by inductively coupled plasma-mass spectrometry (ICP-MS) in the Geochemical Laboratory of the Royal Museum for Central Africa in Tervuren, except Sr which was analyzed by XRF in Berlin.

Sr- and Nd-isotope analyses were carried out in the isotopic geology laboratory of the Royal Museum for Central Africa. A detailed description of procedures and measurements is given in Küster and Liégeois (2001). The NBS987 standard yields a value for $^{87}Sr/^{86}Sr$ of 0.710252 ± 0.000010 (2σ on the mean of 20 standards measured together with the samples, normalized to $^{86}Sr/^{88}Sr = 0.1194$) and the MERCK Nd standard a value for $^{143}Nd/^{144}Nd$ of 0.511738 ± 0.000008 (2σ on the mean of 20 standards measured together with the samples, normalized to $^{146}Nd/^{144}Nd = 0.7219$, and corresponding to a La Jolla standard value of 0.511866). Calculation of Nd T_{DM} model ages was done following Nelson and De Paolo (1985).

Pb isotope ratios were determined on whole rock samples at GeoForschungsZentrum Potsdam. Analytical procedures have been described in Romer et al. (2005). Powdered samples were treated with acetic acid to remove any secondary carbonate. The dried samples were dissolved in 52% HF on the hot plate for at least 36 h. After drying, the samples were redissolved in 6N HCl. Pb was separated using standard HBr–HCl ion-exchange chemistry. Pb isotope ratios were measured using static multi-collection on a MAT 262 mass spectrometer at controlled temperatures between 1220 and 1250 °C. The 2σ reproducibility of all Pb isotope ratios of the NBS SRM 981 standard is better than 0.1% and a 2σ error of 0.1% is assumed for the measured samples. Instrumental mass-fractionation has been corrected using 0.1% per a.m.u. on the base of the NBS SRM 981 values. Procedural blanks were <30 pg for Pb and no blank corrections have been applied to the measured ratios because blank contribution were insignificant in comparison to the amount of the respective elements in the sample. Initial Pb isotope compositions have been calculated from U, Th and Pb contents (ICP-MS determinations) and the respective ages of the samples.

Six samples from the Bayuda Desert and Sabaloka region are dated here using the U–Pb on zircon chronometer. Seventy-nine zircon grains were analyzed. The measurements were carried out on a SHRIMP-II ion microprobe at the Centre for Isotopic Research (VSEGEI, St. Petersburg, Russia). Zircon grains were hand selected and mounted in epoxy resin, together with chips of the TEMORA (Middledale Gabbroic Diorite, New South Wales, Australia, age = 417 Ma, Black and Kamo, 2003) and 91,500 (Geostandard zircon, age = 1065 Ma, Wiedenbeck et al., 1995) reference zircons. The grains were sectioned approximately in half and polished. Each analysis consisted of five scans through the mass range; the spot diameter was about 18 μm and the primary beam intensity about 4 nA. The data were reduced in a manner similar to that described by Williams (1998, and references therein), using the SQUID Excel Macro of Ludwig (2000). The Pb/U ratios were normalized relative to a value of 0.0668 for the $^{206}Pb/^{238}U$ ratio of the TEMORA zircon, equivalent to an age of 416.75 Ma (Black and Kamo, 2003). Uncertainties given for individual analyses (ratios and ages) in Table 1 are at the one σ level, whereas uncertainties in calculated concordia ages are reported at the 2σ level. Age calculations were performed using Isoplot 3 Excel macro (Ludwig, 2003).

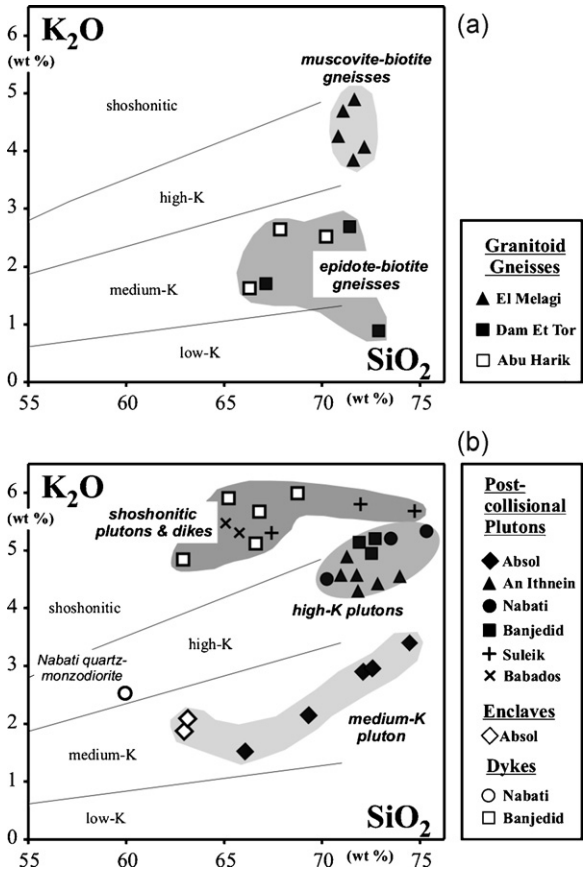

Fig. 4. K_2O vs. SiO_2 plot for (a) granitoid gneisses from Bayuda Desert and (b) post-collisional granitoids from Bayuda Desert and Sabaloka.

5. Geology, petrography and geochemistry of the granitoid suites

5.1. Granitoid gneisses

Regional distribution, petrography, geochemistry and Sr–Nd isotope geochemistry of the metamorphosed granitoids have previously been investigated (Küster and Liégeois, 2001). Only a synopsis of these findings will thus be given here (Table 1). There are two basically different types of granitoid gneisses in the Bayuda Desert: (1) muscovite–biotite gneisses from the Rahaba Series, which occupy large areas in northern and central Bayuda Desert (El Melagi locality; Fig. 3) and (2) epidote–biotite gneisses from the Kurmut Series (eastern Bayuda), which are intimately associated with amphibolites and metasedimentary gneisses (Dam Et Tor locality; Fig. 3).

The muscovite–biotite gneisses from El Melagi are characteristic representatives of the Rahaba Series of Barth and Meinhold (1979) and form a lithologically rather monotonous sequence. These gneisses have the chemistry of high-K granitoids with $SiO_2 > 70\%$ (Fig. 4a). They are strongly peraluminous (A/CNK > 1.15, norm. (normative) corundum > 2%, norm. pyroxene < 1.6%) and their trace-element signature is similar to two-mica granite sheets from the Himalaya collisional chain (Küster and Liégeois, 2001). In the field, the El Melagi muscovite–biotite gneisses often display a thrust-like flat-lying foliation. The El Melagi gneisses could thus represent deformed S-type pelite-derived granites emplaced during a convergent tectonometamorphic event or siliciclastic sediments metamorphosed during such an event.

Table 1
Geological features of granitoid orthogneisses and late- to post-collisional granitoids from Bayuda Desert and Sabaloka

Occurrence	Rock types	Chemistry	SiO_2 (%)	Country rock
Bayuda Desert				
Dam Et Tor				
Gneiss	Epidote–biotite gneiss	Low- to medium-K	65–73	Intercalated with amphibolites, hornblendites and quartzo-feldspathic schists
El Melagi				
Gneiss	Muscovite–biotite gneiss	High-K	73–74	Monotonous succession, partly pegmatized, rare lenses of mica schist and quartzite
Absol				
Pluton	Greyish biotite granite to epidote–biotite granodiorite	Medium-K	66–74	Amphibolite-facies gneisses and schists epidote–biotite granodiorite
Enclaves	Epidote–garnet–hornblende tonalite	Medium-K	63	
Nabati				
Pluton	Reddish biotite granite	High-K	70–76	Low-grade metavolcanosedimentary rocks
Dykes	Quartz–monzodiorite	High-K	60	
An Ithnein				
Pluton	Greyish biotite granite	High-K	70–74	Amphibolite-facies schists
Sabaloka				
Banjedid				
Pluton	Reddish biotite granite	High-K	71–73	Amphibolite-facies gneisses and migmatites
Dykes	Porphyritic biotite granite and hornblende–biotite granite	Shoshonitic	62–69	
Babados				
Pluton	Hornblende–biotite granite	Shoshonitic	65–66	Amphibolite-facies gneisses and migmatites
Suleik				
Pluton	Dark to reddish biotite granite and hornblende–biotite granite	Shoshonitic	67–75	Amphibolite-facies gneisses and migmatites

The epidote–biotite gneisses from Khor Dam Et Tor are low- to medium-K granitoids (Fig. 4a). They are metaluminous to slightly peraluminous (A/CNK 0.85–1.05, norm. pyroxene > 4%, norm. corundum < 0.15%) and their trace-element signatures are akin to subduction-related I-type magmas from relatively primitive oceanic arcs (Küster and Liégeois, 2001). The epidote–biotite gneisses are part of a metavolcanosedimentary succession which include also amphibolites and intermediate to felsic metasediments and paragneisses. The whole succession derived from a subduction-related magmatism in an intra-oceanic arc system dated at 806 ± 19 Ma (Sm–Nd isochron; Küster and Liégeois, 2001). The epidote–biotite gneisses are therefore believed to represent metamorphosed dacites and rhyodacites of this oceanic magmatism. The Dam Et Tor succession would be part of the Absol Series of Barth and Meinhold (1979). However, the lithological succession identified by us along Khor Dam Et Tor is dominated by metavolcanics and as such much more akin to Barth and Meinhold's Kurmut Series (see Section 3.1). We have therefore included the Dam Et Tor succession into the Kurmut Series and modified the map (Fig. 3) accordingly. Epidote–biotite gneisses of similar geochemistry also occur in the southeastern part of the Bayuda Desert where they are part of the Abu Harik Series of Barth and Meinhold (1979). However, these gneisses are not interrelated with amphibolites and rather appear metaplutonic. They are outlined on the map (Fig. 3) as syn-tectonic intrusives.

5.2. Granitoid plutons

Post-collisional granitoids occur in discordant crosscutting plutons in the Bayuda Desert and at Sabaloka. The location of the investigated occurrences is shown in Fig. 3. The plutons usually consist of grey to reddish biotite granite and of subordinate biotite–hornblende granite and granodiorite. Petrochemically, they are distinguished into calc-alkaline medium-K, high-K and shoshonitic suites (Table 2, Fig. 4b). The term shoshonitic is used here to describe granitoids with a 'very high-K' character. Although shoshonitic has been initially defined for volcanic rocks, it has also become a common practice to use this term also for granitoids (cf. Liégeois et al., 1998; Duchesne et al., 1998). Most of the post-collisional plutons in the study area display only limited geochemical and petrographical variations; only the Absol, Banjedid and Nabati plutons show greater differences due to presence of melanocratic enclaves or crosscutting dykes. A brief overview about geological characteristics and geochemical composition is supplied in Tables 1 and 2. Individual plutons will be discussed in more detail below.

5.2.1. Absol medium-K pluton

The Absol pluton is an oval shaped intrusion in the northeastern Bayuda Desert intrusive into the Absol Series (Fig. 3). It is composed of medium to coarse grained, equigranular to slightly porphyritic greyish biotite granite and granodiorite. Both may contain rounded melanocratic enclaves of tonalitic composition. The granodiorites are epidote bearing and the enclaves are made up of hornblende–garnet–epidote tonalite. Although the Absol pluton appears undeformed, the occurrence of epidote and garnet in these rocks indicates a metamorphic overprint. Together with its oval shape, this suggests that the Absol pluton has been incorporated in transcurrent tectonics in which it behaved as a rigid body. The Absol should then be better described as a metapluton corresponding to a boudin parallel to the regional structural trend, as for example the Follum metapluton in Norway (Bingen et al., 2005).

The Absol pluton has a medium-K calc-alkaline composition (Fig. 4b) and an extended silica range (63–74%). ORG-normalized incompatible element signatures (not shown) are akin to subduction-related magmatism at continental arc settings (e.g. rhyolites from northern Chile volcanic zone) or to granites from continent–arc or continent–continent collision zones (e.g. Oman or Pyrenees). The existence of tonalitic magmatic enclaves indicates

Table 2
Major and trace-element geochemistry of selected samples of late- to post-collisional granitoids

	Medium-K granitoids				High-K granitoids							Shoshonitic granitoids					
	Absol pluton				An Ithnein pluton			Nabati pluton		Banjedid pluton		Banjedid dykes			Babados	Suleik pluton	
	10-8b[a] *enclave*	10-8a[a]	10-7e[a]	10-6[a]	14-3[a] *porph.*	14-5[a] *equigr.*	14-7[a] *equigr.*	15-2[a]	15-1[a] *dyke*	18-8[a]	17-4b[a]	17-4f[a]	18-1b[a]	18-1c[a]	18-5a[a]	18-7[a]	18-6b[a]
wt. %																	
SiO_2	62.97	69.18	72.86	74.35	70.88	71.71	74.38	73.04	60.01	72.54	71.93	62.29	66.76	69.26	65.81	72.55	75.13
Al_2O_3	16.25	15.98	14.34	13.74	15.04	14.81	14.07	13.84	15.02	14.68	14.41	14.41	15.03	14.64	14.69	13.67	12.96
Fe_2O_3	5.55	3.30	2.06	1.91	2.84	1.46	0.96	1.84	8.46	1.29	0.82	7.07	3.97	2.78	5.99	2.82	1.22
MnO	0.13	0.07	0.06	0.05	0.04	0.03	0.02	0.02	0.11	0.01	0.01	0.07	0.02	0.01	0.05	0.03	0.01
MgO	2.27	1.23	0.69	0.40	0.60	0.53	0.08	0.31	2.54	0.24	0.19	1.29	0.84	0.67	1.03	0.33	0.17
CaO	4.80	3.84	2.61	1.71	1.88	1.59	0.61	1.23	5.21	1.73	1.65	3.45	2.18	1.61	2.70	1.47	1.35
Na_2O	3.48	3.73	3.61	3.51	3.94	4.28	4.29	3.55	3.88	3.53	3.41	2.96	3.04	2.94	2.69	2.74	2.84
K_2O	2.18	2.41	3.15	3.51	4.58	4.17	4.68	5.15	2.43	4.96	5.08	4.81	5.65	6.15	5.18	5.80	5.49
TiO_2	0.75	0.42	0.27	0.20	0.45	0.26	0.10	0.37	2.07	0.24	0.15	1.73	0.98	0.62	1.31	0.37	0.21
P_2O_5	0.35	0.14	0.13	0.08	0.15	0.09	0.04	0.09	0.91	0.03	0.01	0.68	0.30	0.19	0.53	0.12	0.06
LOI	0.87	0.64	0.47	0.59	0.82	1.10	0.52	0.81	0.80	0.74	0.70	0.84	0.97	0.71	0.84	0.80	0.77
SUM	99.60	100.94	100.25	100.05	101.22	100.03	99.75	100.25	101.44	99.99	98.36	99.60	99.74	99.58	100.82	100.70	100.21
ppm																	
Sr	366	314	234	161	295	323	78	167	652	391	353	249	178	141	256	140	185
Ba	290	420	425	514	881	762	328	951	1009	1380	788	993	985	811	1099	642	613
Rb	93	79	84	123	164	136	186	66	59	84	160	318	226	389	220	320	223
Zr	155	133	80	94	269	118	99	279	516	144	103	987	785	470	787	337	252
Y	19.44	12.16	13.18	20.19	24.51	6.58	9.98	8.67	29.32	3.23	1.24	43.83	12.94	11.23	34.42	21.22	8.51
Th	8.93	8.61	6.77	11.53	25.79	13.13	20.39	8.40	12.50	7.52	17.58	43.79	147.36	97.23	46.92	59.60	19.41
U	4.08	3.66	3.57	2.31	6.95	2.48	15.03	2.33	3.31	2.04	0.98	1.19	4.52	2.24	2.06	12.21	2.10
Pb	16.08	17.62	22.93	25.66	22.18	21.34	29.46	13.81	14.39	34.14	35.75	37.15	36.00	42.75	28.92	38.82	30.33
Hf	4.35	3.96	2.67	3.14	7.60	3.76	4.61	7.65	13.08	4.82	3.16	23.87	22.62	10.77	22.23	8.73	6.69
Nb	16.30	7.42	6.74	7.59	11.74	3.40	13.07	6.36	18.11	4.67	2.49	34.92	18.21	10.34	28.78	14.22	8.17
Ta	1.36	0.68	0.82	0.75	1.37	0.37	1.13	0.38	1.09	0.31	0.04	1.42	0.84	0.26	1.37	0.17	0.25
La	56.18	27.25	16.57	26.67	54.94	20.10	20.81	84.57	94.07	23.19	23.01	145.85	248.88	180.52	135.74	104.41	88.86
Ce	100.03	54.38	37.31	61.63	110.13	37.81	40.88	154.02	206.65	40.89	38.40	331.47	529.27	368.23	309.29	224.97	159.72
Pr	12.58	6.00	3.71	6.27	11.99	4.21	5.09	15.52	24.86	4.42	3.73	40.40	60.69	38.49	38.24	24.56	15.41
Nd	47.70	21.84	14.10	23.21	43.85	15.38	19.82	50.90	99.80	16.29	10.84	143.78	218.35	111.79	154.65	75.37	43.00
Eu	1.47	1.01	0.81	0.68	1.16	0.66	0.66	1.42	3.61	0.84	0.56	2.16	2.01	0.80	2.83	1.03	1.45
Sm	7.27	3.73	2.98	4.60	7.66	2.65	4.39	6.10	16.57	2.60	1.00	22.26	27.45	12.96	26.34	11.52	4.78
Gd	5.50	3.06	2.71	4.06	6.13	1.87	3.31	4.02	12.13	1.73	0.69	13.94	15.04	6.89	17.57	7.60	2.66
Dy	3.54	2.29	2.34	3.61	4.53	1.20	2.07	1.71	6.80	0.78	0.33	8.24	4.01	1.99	9.06	4.30	1.55
Ho	0.69	0.43	0.44	0.72	0.85	0.22	0.36	0.32	1.17	0.11	0.05	1.38	0.56	0.29	1.50	0.66	0.27
Er	1.88	1.17	1.25	2.07	2.35	0.62	0.97	0.98	2.88	0.30	0.13	2.70	1.51	0.47	3.56	1.31	0.53
Yb	1.87	1.06	1.21	1.91	2.15	0.59	0.92	1.01	2.13	0.28	0.17	1.99	1.45	0.51	2.35	0.85	0.57
Lu	0.27	0.15	0.15	0.26	0.29	0.08	0.12	0.15	0.28	0.03	0.02	0.25	0.17	0.09	0.30	0.13	0.08

[a] Sample.

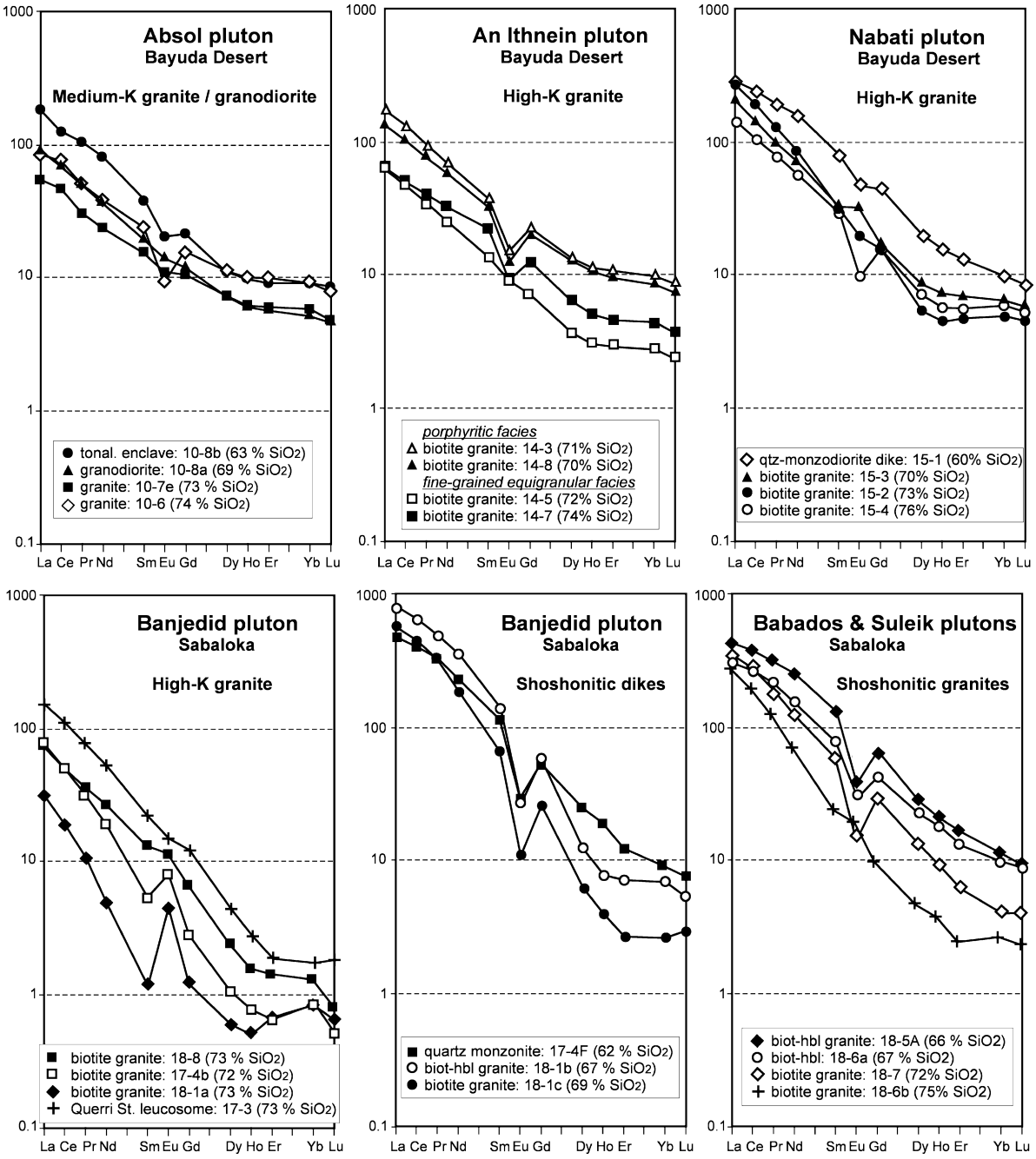

Fig. 5. Chondrite normalized REE patterns for medium-K, high-K and shoshonitic granitoids from Bayuda Desert and Sabaloka.

the contemporaneous intrusion of at least two different magmas. REE data (Table 2, Fig. 5) reveal that the tonalitic enclaves have the highest REE contents ($\sum$REE > 200 ppm) and the most fractionated patterns ($La_N/Yb_N = 20$) with moderate Eu anomalies ($Eu/Eu^* = 0.7$), while granodiorites and most granites are less enriched ($\sum$REE = 80–120 ppm) and have less fractionated patterns ($La_N/Yb_N = 9–12$) with negligible Eu anomalies ($Eu/Eu^* = 0.9–1.0$). Only the most siliceous granite displays again an enrichment in total REE ($\sum$REE = 135 ppm) and a significant Eu anomaly ($Eu/Eu^* = 0.5$). The REE pattern of individual phases of the Absol pluton (tonalitic enclaves, highly silicic granitoids, granodiorites and moderately silicic granites) are difficult to relate to each other by a magmatic fractionation process. It seems therefore likely that the Absol pluton represent a composite intrusion with magmas derived from different sources and/or from magma mixing or contamination.

5.2.2. An Ithnein, Nabati and Banjedid high-K plutons

Discordant circular shaped plutons of high-K calc-alkaline biotite granite occur in both Bayuda Desert and Sabaloka. Three of these plutons were investigated (see also Table 1):

(1) the An Ithnein pluton intrusive into the Rahaba Series (Fig. 3), made up of greyish biotite granite;
(2) the Nabati pluton intrusive into the Kurmut Series (Fig. 3), composed of reddish biotite granite and crosscut by dykes of quartz monzodioritic composition;

(3) the Banjedid pluton from Sabaloka (Fig. 3), composed of reddish biotite granite and crosscut by dikes of granitic to quartz monzonitic composition.

These high-K biotite granites are all silica-rich (>70% SiO_2), while the crosscutting dykes often show more mafic compositions (Fig. 4b). The Nabati quartz–monzodiorite dyke has ~60% SiO_2 and is also high-K calc-alkaline in composition. The Banjedid dykes have 62–69% SiO_2 and are all shoshonitic in composition (Fig. 4b).

Although the high-K granites are clearly post-kinematic and undeformed, incompatible trace-element spidergrams (not shown) are akin to subduction-related continental margin rhyolites and rhyodacites (e.g. from Chile central volcanic zone). This is interpreted here not as an active subduction regime, but as a characteristic of the source which was tapped during the post-collisional period. This implies that a subduction period occurred earlier in the region, for instance at ca. 800 Ma, the age of the Bayuda island arc (Küster and Liégeois, 2001).

5.2.2.1. An Ithnein pluton (Rahaba Series). The An Ithnein pluton has a narrow SiO_2 span (70–74%) but contains two magmatic varieties: a medium-grained equigranular granite and a coarse-grained porphyritic granite. The equigranular biotite granite has higher Na_2O and lower Fe_2O_3, TiO_2, P_2O_5, Rb, and HFSE (Zr, Nb, Y) than the porphyritic biotite granite (Table 2). The equigranular granite also has low $\sum$REE (85–107 ppm) and displays only minor Eu anomalies ($Eu/Eu^* = 0.9$) while the porphyritic granite has higher $\sum$REE (195–246 ppm) and displays significant Eu anomalies ($Eu/Eu^* = 0.35–0.52$). The most siliceous granite of the An Ithnein pluton (sample 14-7, Table 2) is geochemically close to the equigranular granite, but it is more evolved and shows a negative Eu anomaly (Fig. 5). The An Ithnein pluton is likely to be derived from at least two compositionally slightly different high-K magmas.

5.2.2.2. Nabati pluton (Kurmut Series). The Nabati pluton is composed of coarse-grained reddish biotite granite with SiO_2 values in the range 70–76%. With increasing silica content there is a decrease in Al_2O_3, Fe_2O_3, CaO, Na_2O, TiO_2, P_2O_5, Sr, Ba and Zr, while K_2O and Rb are enriched. The REE patterns are characterized by different types of Eu anomalies (Fig. 5), which change with increasing silica from positive ($Eu/Eu^* = 1.35$) to negative anomalies ($Eu/Eu^* = 0.46$). The negative Eu anomaly together with the characteristic trace and major element variation indicate that the granite magma has experienced magmatic fractionation dominated by feldspar. The positive Eu anomaly in the less siliceous sample (15-3, Fig. 5) may indicate either cumulus plagioclase or restitic plagioclase entrained as a solid phase in the melt during its generation. The Nabati biotite granite is cut by dykes of quartz monzodioritic (norm. Q'-ANOR) or granodioritic (norm. Ab-An-Or) composition, depending on the classification scheme used. The dykes are moderately potassic (2.5% K_2O at 60% SiO_2) and relatively enriched in HFSE ($TiO_2 = 2.07\%$, Zr = 516 ppm, $\sum$REE = 471 ppm). The REE pattern (Fig. 5) is moderately fractionated ($La_N/Yb_N = 30$, $Eu/Eu^* = 0.78$) and has some similarities with silica-poor samples of the shoshonitic granitoids (discussed further below). ORG-normalized trace-element spidergrams are also close to post-collisional shoshonitic andesites from the Tibetan plateau (not shown). We tentatively consider the Nabati quartz monzodiorite as a fractionated mantle melt which may have largely been derived from a calc-alkaline high-K basaltic parent.

5.2.2.3. Banjedid pluton (Sabaloka region). The Banjedid pluton is composed of slightly reddish medium- to coarse-grained equigranular biotite granite. It has a very narrow silica range (71.7–72.6% SiO_2) and consequently does not show much geochemical variation (Table 2). REE contents are low ($\sum$REE = 31–91 ppm), but due to very low HREE content, the patterns are fractionated ($La_N/Yb_N = 31–91$) and typically characterized by positive Eu anomalies ($Eu/Eu^* = 1.2–3.8$). The latter feature may again be interpreted as restitic or early crystallized plagioclase entrained in the melt during its generation, most likely in the continental crust. The very low HREE contents argue for a dominant role of garnet in the restite. The Banjedid high-K granite pluton is cut by granitoid dykes of shoshonitic composition which will be discussed together with shoshonitic plutons in the next chapter.

5.2.3. Babados, Suleik and Banjedid shoshonitic plutons and dykes (Sabaloka region)

Shoshonitic granitoids are abundant only at Sabaloka and occur in discordant plutons and as crosscutting dykes. Three of these occurrences were investigated:

(1) the Babados pluton (Fig. 3), composed of medium-grained slightly porphyritic melanocratic hornblende–biotite granite and quartz monzonite;
(2) the Suleik pluton (Fig. 3), composed of porphyritic coarse-grained hornblende–biotite granite and medium-grained reddish biotite granite;
(3) dykes within the (high-K) Banjedid pluton, made up of fine- to medium-grained, equigranular to porphyritic melanocratic quartz monzonite and hornblende–biotite granite.

The shoshonitic granitoid rocks are classified as quartz monzonite and granite in Ab-An-Or normative triangle, and as mainly monzogranite and granite in Q'ANOR normative diagram. Most of the rocks typically display magmatic alignment of K-feldspar porphyroblasts. The granitoids are generally low in silica (<70% SiO_2), only the Suleik pluton contains more silicic rocks transitional to high-K granites (Fig. 4b). ORG-normalized trace-element spidergrams (not shown) are remarkably similar to post-collisional shoshonitic rhyolites and rhyodacites from the Tibetan plateau.

The shoshonitic granitoids are enriched in REE ($\sum$REE = 320–1109 ppm) and other HFSE (Table 2). The REE patterns (Fig. 5) are highly fractionated ($La_N/Yb_N = 39–240$) and all samples show distinct Eu anomalies ($Eu/Eu^* = 0.52–0.26$), only the most silica rich granite from Suleik pluton (sample 18-6b, Table 2) has a different pattern ($Eu/Eu^* = 1.26$) and appears transitional to the Banjedid high-K granite. Based on REE data, a generation of the low-silica granitoids of this group (62–67% SiO_2) may be explained by fractional crystallization of feldspar ± hornblende and accessories from a more mafic melt. Further fractionation, especially of accessories (apatite, zircon), could then be responsible for the depletion of REE in the more siliceous granites (69–72% SiO_2) of the shoshonitic group, except sample 18-6b (Fig. 5).

6. Geochronology

6.1. Rahaba and Absol Series

Three samples have been dated out of the Rahaba and Absol Series: the amphibolite-facies El Melagi Ms-Bi gneiss (sample 12-2), the Absol metapluton (sample 10-8A) and the An Ithnein pluton (sample 14-3). Results of SHRIMP-II ion microprobe U-Pb measurements are shown in Table 3. Cathodoluminescence pictures of the dated zircons are given in Fig. 6 and Concordia diagrams in Fig. 7.

Twelve zircons from the El Melagi gneiss have been dated. These zircons are variably elongated, often zoned and comprise inherited cores sometimes well rounded (8.1). Some zircons display cores inside cores: core 8.1 contains the older zoned core 8.2 (Fig. 6). These cores are large and the rims are often thin and, unfortunately,

Table 3
SHRIMP U–Pb zircon results of granitoid rocks from Bayuda Desert and Sabaloka

Grain spot	$^{206}Pb_c$ %	U (ppm)	Th (ppm)	$^{232}Th/^{238}U$	$^{206}Pb^*$ (ppm)	$^{206}Pb/^{238}U^*$[a], Age (Ma)	$^{207}Pb/^{206}Pb^*$[a], Age (Ma)	% Disc.	$^{207}Pb^*/^{206}Pb^*$[a], ±%	$^{207}Pb^*/^{235}U$[a], ±%	$^{206}Pb^*/^{238}U$[a], ±%	Err corr
Dam Et Tor gneiss 11-2A												
11-2A.1.1	0.90	150	76	0.52	17.4	809, ±18	780, ±320	−4	0.0650, 15	1.200, 16	0.1337, 2.3	0.149
11-2A.2.1	0.54	99	43	0.44	11.4	803, ±18	788, ±96	−2	0.0654, 4.6	1.196, 5.2	0.1326, 2.4	0.470
11-2A.3.1	0.10	154	29	0.19	18.9	859, ±9.0	826, ±46	−4	0.0666, 2.2	1.310, 2.5	0.1426, 1.1	0.452
11-2A.3.2	0.09	33	12	0.37	4.12	886, ±19	899, ±100	1	0.0690, 5.0	1.401, 5.5	0.1473, 2.3	0.414
11-2A.4.1	0.25	159	31	0.20	20.0	882, ±20	845, ±76	−4	0.0672, 3.7	1.359, 4.4	0.1465, 2.4	0.544
11-2A.5.1	0.18	110	41	0.39	13.6	865, ±9.8	818, ±63	−5	0.0664, 3.0	1.313, 3.2	0.1435, 1.2	0.375
11-2A.6.1	0.49	79	34	0.45	9.38	832, ±11	811, ±110	−2	0.0662, 5.3	1.256, 5.5	0.1377, 1.4	0.250
11-2A.7.1	0.35	91	35	0.40	11.1	857, ±10	813, ±91	−5	0.0662, 4.3	1.299, 4.5	0.1423, 1.3	0.287
11-2A.8.1	0.06	134	61	0.47	16.5	858, ±9.2	847, ±38	−1	0.0673, 1.8	1.321, 2.2	0.1424, 1.1	0.530
11-2A.9.1	0.35	142	65	0.47	17.3	855, ±9.1	851, ±69	0	0.0674, 3.3	1.319, 3.5	0.1418, 1.1	0.326
11-2A.10.1	0.32	108	51	0.49	13.5	873, ±15	876, ±62	0	0.0682, 3.0	1.364, 3.5	0.1450, 1.8	0.522
El Melagi gneiss 12-2												
12.2.1.1	0.14	663	263	0.41	78.2	829, ±6.3	987, ±20	16	0.0721, 1.0	1.363, 1.3	0.1372, 0.8	0.629
12.2.7.2	0.03	932	25	0.03	120	898, ±6.6	928, ±16	3	0.0699, 0.8	1.443, 1.1	0.1495, 0.8	0.718
12.2.8.1	0.03	682	43	0.06	87.8	900, ±6.8	926, ±17	3	0.0699, 0.8	1.444, 1.2	0.1499, 0.8	0.703
12.2.2.1	0.03	4136	189	0.05	554	934, ±6.5	918, ±7.7	−2	0.0696, 0.4	1.497, 0.8	0.1559, 0.7	0.892
12.2.6.1	0.18	433	157	0.38	57.2	920, ±7.3	857, ±32	−7	0.0676, 1.5	1.431, 1.8	0.1534, 0.9	0.489
12.2.8.2	0.26	199	122	0.63	30.8	1065, ±9.8	1033, ±40	−3	0.0737, 2.0	1.826, 2.2	0.1797, 0.9	0.454
12.2.4.1	0.06	426	188	0.46	132	1989, ±24	2460, ±9.4	19	0.1604, 0.6	7.990, 1.5	0.3614, 1.4	0.928
12.2.4.2	0.02	190	51	0.28	75.1	2436, ±22	2525, ±18	4	0.1667, 1.0	10.55, 1.5	0.4591, 1.1	0.725
12.2.3.2	0.23	51	41	0.82	21.4	2543, ±29	2647, ±20	4	0.1793, 1.2	11.96, 1.8	0.4836, 1.4	0.761
12.2.3.1	0.01	489	52	0.11	210	2614, ±20	2664, ±17	2	0.1812, 1.0	12.49, 1.4	0.5001, 0.9	0.671
12.2.7.1	0.13	251	102	0.42	50.8	1363, ±21	1850, ±21	26	0.1131, 1.1	3.673, 2.1	0.2355, 1.7	0.834
12.2.5.1	0.03	798	307	0.40	238	1922, ±13	1978, ±7.4	3	0.1215, 0.4	5.817, 0.9	0.3473, 0.8	0.883
Absol pluton 10-8A												
10-8A.7.1	0.92	1078	135	0.13	98.7	647, ±6.0	889, ±51	37	0.0687, 2.5	0.999, 2.6	0.1055, 1.0	0.366
10-8A.1.1	0.73	2019	273	0.14	213	743, ±5.6	899, ±20	21	0.0690, 1.0	1.162, 1.3	0.1221, 0.8	0.637
10-8A.3.1	0.05	3616	334	0.10	423	823, ±6.0	901, ±9.2	10	0.0691, 0.5	1.296, 0.9	0.1361, 0.8	0.868
10-8A.8.1	0.28	610	108	0.18	72.0	828, ±6.8	914, ±26	10	0.0695, 1.3	1.313, 1.5	0.1370, 0.9	0.571
10-8A.5.1	0.16	389	53	0.14	46.3	836, ±7.9	920, ±35	10	0.0697, 1.7	1.331, 2.0	0.1385, 1.0	0.515
10-8A.6.1	0.07	468	59	0.13	59.0	883, ±8.2	917, ±23	4	0.0696, 1.1	1.409, 1.5	0.1468, 1.0	0.669
10-8A.4.1	0.14	417	51	0.13	54.5	911, ±8.1	870, ±32	−5	0.0680, 1.5	1.424, 1.8	0.1518, 1.0	0.527
10-8A.2.1	0.05	366	87	0.24	47.4	905, ±7.7	892, ±24	−1	0.0688, 1.2	1.430, 1.5	0.1508, 0.9	0.617
An Ithnein pluton 14-3												
14-3.7.1	1.19	593	256	0.45	30.5	371, ±3.7	695, ±68	87	0.0626, 3.2	0.512, 3.4	0.0593, 1.0	0.304
14-3.9.1	1.44	517	150	0.30	39.8	546, ±4.7	694, ±77	27	0.0626, 3.6	0.762, 3.7	0.0883, 0.9	0.239
14-3.2.1	1.67	465	176	0.39	36.9	561, ±5.6	598, ±86	7	0.0599, 4.0	0.750, 4.1	0.0909, 1.0	0.254
14-3.1.1	0.26	616	173	0.29	50.3	584, ±5.6	573, ±35	−2	0.0592, 1.6	0.773, 1.9	0.0948, 1.0	0.528
14-3.10.1	0.56	802	173	0.22	66.3	590, ±5.3	565, ±36	−4	0.0590, 1.7	0.778, 1.9	0.0957, 0.9	0.489
14-3.3.1	0.79	312	89	0.30	26.2	596, ±6.4	640, ±73	7	0.0610, 3.4	0.815, 3.6	0.0969, 1.1	0.312
14-3.6.1	0.04	1574	254	0.17	131	597, ±5.0	610, ±16	2	0.0602, 0.7	0.805, 1.1	0.0970, 0.9	0.770
14-3.7.2	0.07	315	212	0.69	26.6	604, ±5.4	602, ±31	0	0.0599, 1.4	0.811, 1.7	0.0982, 0.9	0.546
14-3.8.1	–	271	67	0.25	22.9	606, ±6.6	603, ±44	0	0.0600, 2.0	0.815, 2.3	0.0986, 1.1	0.494
14-3.4.1	0.33	203	103	0.52	17.3	609, ±6.2	583, ±82	−4	0.0594, 3.8	0.812, 3.9	0.0991, 1.1	0.273
14-3.5.1	0.06	302	124	0.42	26.6	629, ±5.7	603, ±36	−4	0.0600, 1.7	0.847, 1.9	0.1025, 1.0	0.494
Banjedid pluton 18-8												
18.8.4.1	1.13	890	145	0.17	70.7	564, ±4.5	621, ±54	9	0.0605, 2.5	0.763, 2.6	0.0915, 0.8	0.318
18.8.4.2	0.01	3161	54	0.02	256	581, ±4.2	626, ±11	7	0.0606, 0.5	0.789, 0.9	0.0944, 0.8	0.826
18.8.1.2	0.01	2214	65	0.03	181	585, ±4.3	607, ±15	4	0.0601, 0.7	0.787, 1.0	0.0950, 0.8	0.745
18.8.6.1	0.03	1964	323	0.17	161	586, ±4.4	599, ±15	2	0.0599, 0.7	0.785, 1.0	0.0951, 0.8	0.742
18.8.2.1	0.11	731	88	0.12	61.5	601, ±4.7	576, ±27	−4	0.0593, 1.2	0.798, 1.5	0.0977, 0.8	0.551
18.8.5.2	0.05	2610	65	0.03	220	602, ±4.4	590, ±14	−2	0.0596, 0.6	0.805, 1.0	0.0979, 0.8	0.772
18.8.7.1	0.34	1043	155	0.15	89.1	609, ±5.2	565, ±35	−8	0.0589, 1.6	0.805, 1.9	0.0991, 0.9	0.483
18.8.5.1	0.05	349	36	0.11	29.8	610, ±5.5	589, ±39	−4	0.0596, 1.8	0.816, 2.0	0.0993, 0.9	0.468
18.8.1.1	0.09	1091	110	0.10	93.4	612, ±4.7	589, ±25	−4	0.0596, 1.2	0.818, 1.4	0.0996, 0.8	0.567
18.8.3.1	0.43	378	39	0.11	33.9	638, ±6.6	540, ±72	−18	0.0583, 3.3	0.836, 3.4	0.1040, 1.1	0.314
Babados pluton 18-5A												
18.5A.1.2	0.08	561	168	0.31	46.4	592, ±4.9	600, ±28	1	0.0599, 1.3	0.794, 1.6	0.0962, 0.9	0.561
18.5A.3.2	0.06	603	184	0.31	50.1	594, ±4.8	621, ±35	4	0.0605, 1.6	0.805, 1.8	0.0966, 0.8	0.461
18.5A.4.2	0.27	587	423	0.75	48.6	592, ±4.8	488, ±36	−21	0.0569, 1.6	0.754, 1.8	0.0961, 0.8	0.457
18.5A.1.1	1.02	75	82	1.14	6.32	601, ±9.0	294, ±270	−104	0.0522, 12	0.703, 12	0.0977, 1.6	0.134
18.5A.2.1	0.18	337	330	1.01	27.7	590, ±5.5	603, ±53	2	0.0600, 2.4	0.792, 2.6	0.0958, 1.0	0.371
18.5A.3.1	0.61	105	131	1.29	8.80	597, ±7.5	499, ±120	−20	0.0572, 5.6	0.765, 5.7	0.0970, 1.3	0.229
18.5A.4.1	0.37	111	128	1.18	9.41	602, ±7.1	662, ±93	9	0.0617, 4.3	0.832, 4.5	0.0979, 1.2	0.275
18.5A.5.1	0.20	189	212	1.16	15.7	593, ±6.0	575, ±57	−3	0.0592, 2.6	0.786, 2.8	0.0963, 1.1	0.375
18.5A.6.1	0.00	225	341	1.57	18.1	576, ±7.9	710, ±34	19	0.0631, 1.6	0.812, 2.2	0.0934, 1.4	0.666
18.5A.7.1	0.23	258	339	1.36	21.0	583, ±5.7	622, ±63	6	0.0605, 2.9	0.790, 3.1	0.0947, 1.0	0.329

Errors are 1-sigma; Pb_c and Pb^* indicate the common and radiogenic portions, respectively. Error in Standard calibration was 0.19%.
[a] Common Pb corrected using measured ^{204}Pb.

too thin to be dated. Some grains do not bear cores and are well zoned (3.1; 1.1). The results covered a large spectrum of ages from 900 Ma to the Archaean. It is thus important to consider what kinds of zircons have been dated. The Archaean ages are given by two crystals that have been measured two times each: the two analyses of crystal 3 (3.1 and 3.2) are slightly discordant (2 and 4% discordance); they define a discordia age of 2675 ± 33 Ma when forced through 920 Ma (see below) with an MSWD of 0.0009. One of the two analyses of crystal 4 (4.1 and 4.2) is slightly discordant (4% discordance) while the other is more discordant (19%); they define a discordia age of 2536 ± 45 Ma with a lower intercept of 500 ± 270 Ma. The core 5.1 is also slightly discordant (3%) and gives a $^{207}Pb/^{206}Pb$ age of 1978 ± 15 Ma. The core 7.1 is strongly discordant (26%) and gives a $^{207}Pb/^{206}Pb$ age of 1850 ± 41 Ma; considering its high degree of discordance, not much weight is given to this age: this core could actually have crystallized at ca. 1980 Ma as core 5.1. The last core is concordant (8.2) and provides a Concordia age of 1067 ± 17 Ma (MSWD of concordance = 0.65). Several of these cores are rimmed by zircon (2.1; 7.2; 8.1) having very low Th/U (0.03–0.06), typical of a crystallization in metamorphic conditions (Williams et al., 1996). Two of them are nearly concordant and give an age of 903 ± 9 Ma (MSWD of concordance = 4.5) and the three define a discordia with an upper intercept of 921 ± 10 Ma (MSWD = 0.021). Considering that the two subconcordant rims are slightly to the right of the Concordia, we consider the age of 921 ± 10 Ma as the better approximate for the crystallization of these metamorphic

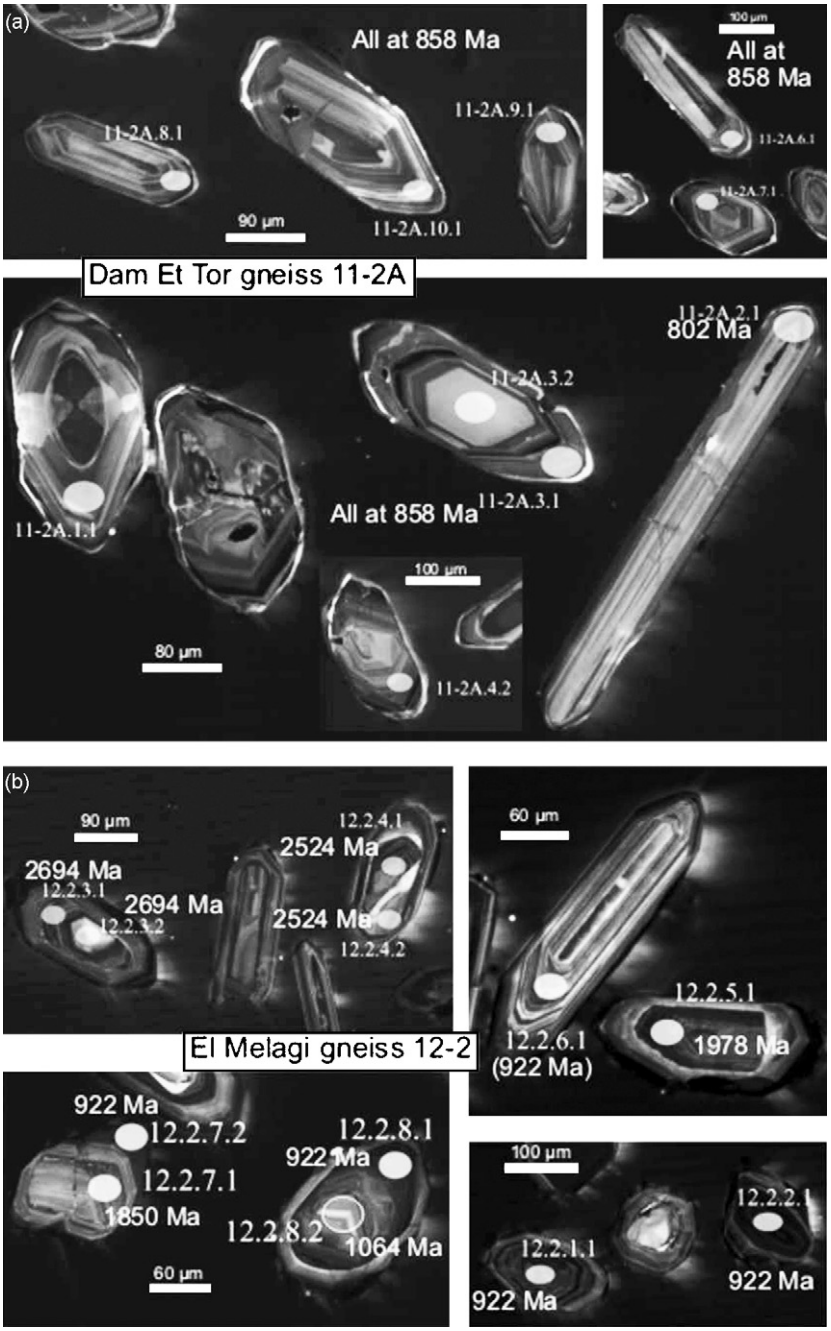

Fig. 6. Cathodoluminescence photographs of dated zircons; (a) Dam Et Tor epidote–biotite gneiss, (b) El Melagi muscovite–biotite gneiss, (c) Absol medium-K pluton, (d) An Ithnein high-K pluton, (e) Banjedid high-K pluton and (f) Babados shoshonitic pluton. See text for further explanation.

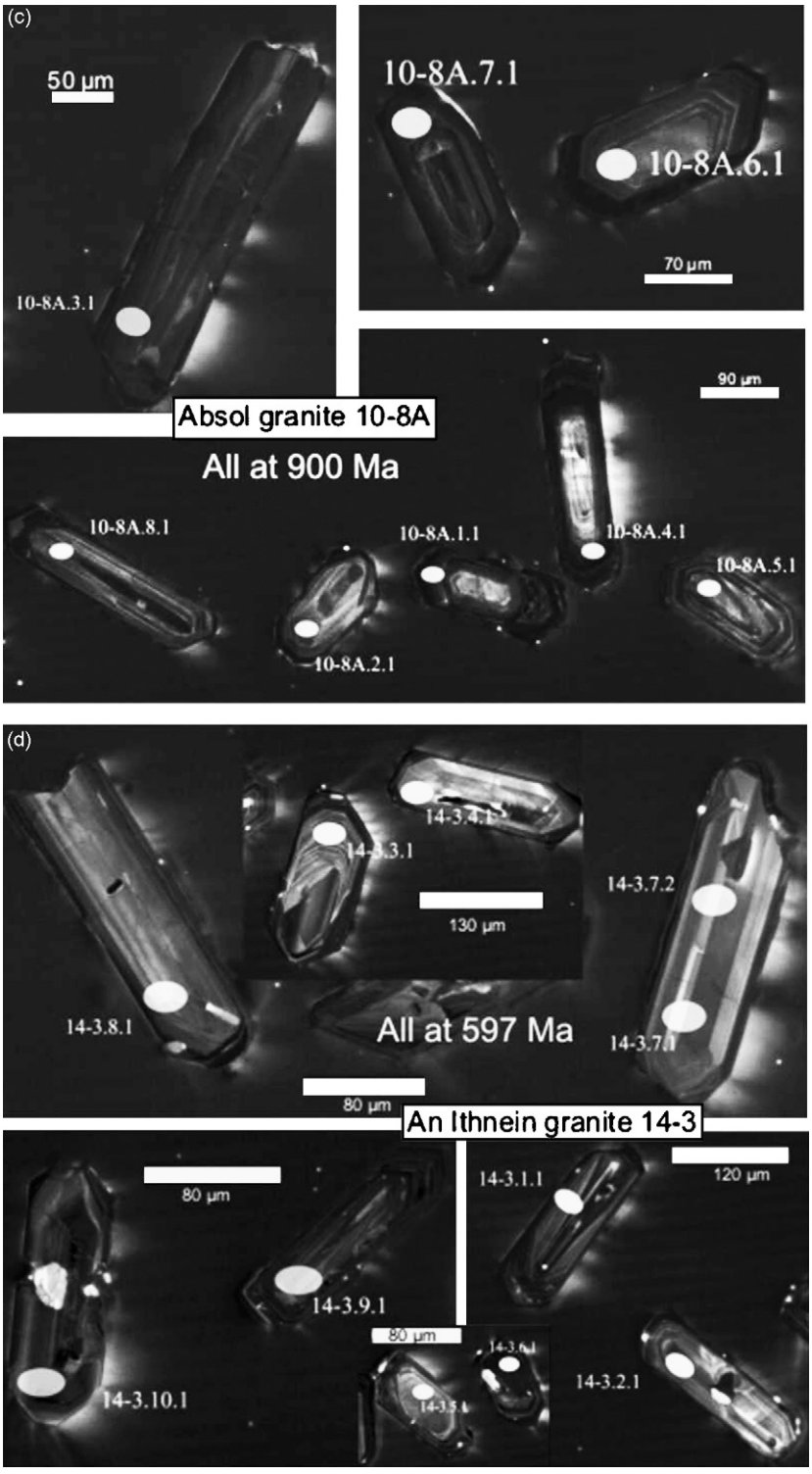

Fig. 6. (*Continued*)

zircon overgrowths. It must be emphasized that these metamorphic rims have grown on 1850 Ma old core (7.2 over 7.1) and on 1064 Ma old core (8.1 over 8.2) but have also grown as individual crystals (2.1). The fact that the latter seems to be rimmed by another rim suggests that an event younger than 920 Ma could have affected this rock. Finally, two zoned zircons without core and with high Th/U (1.1 and 6.1) are more complex to interpret. Zircon 1.1 is strongly discordant (16%) and nothing robust can be interpreted from that analysis: location to the right of the metamorphic discordia line could suggest that it corresponds to a ca. 1064 Ma zircon affected by Pb loss. Zircon 6.1 is an elongated crystal clearly of magmatic origin; it is slightly above the Concordia (−7% discordance) but a Concordia age of 917 ± 14 Ma can be calculated. This age corresponds to the age of the metamorphic overprint. Depending on the nature of the El Melagi gneiss the zircon results indicate that, in the case of an orthogneiss, its pro-

Fig. 6. (*Continued*).

tolith has been metamorphosed soon (<10 m.y.) after its intrusion or, if it is a paragneiss, the age corresponding to the main metamorphism that has affected this rock. In both cases, the zircon data indicate that an amphibolite-facies metamorphism affected the Rahaba Series at ca. 920 Ma. The supracrustal character of the gneiss precursor is confirmed by the abundance of inherited zircons present as cores with ages at ca. 1060, 1980, 2540 and 2675 Ma. These inherited cores demonstrate the presence of Palaeoproterozoic and Archaean material in the sedimentary source region. It is thus concluded that the El Melagi gneiss was metamorphosed at ca. 920 Ma during an amphibolite-facies metamorphic phase that was able to recrystallize zircons. A younger undated event (very thin outer zircon rims) could eventually have affected this rock.

Eight zircons from the Absol granite 10-8A have been analyzed. The zircon crystals are strongly zoned (Fig. 7) and no inherited cores have been clearly identified. Three concordant zircons define a Concordia age at 900 ± 9 Ma (MSWD = 0.02). The other analyses are discordant but form a discordia line giving the same age (901 +25/−19 Ma) with a lower intercept at 0 Ma, suggesting Pb loss. These zircons have a magmatic appearance but relatively low Th/U ratios (0.10–0.24), yet not as low as typical metamorphic zircons (<0.05). We interpret these low values as a result of syn-magmatic competition for U and Th between zircon and other accessory phases with high Kd's for Th such as monazite or allanite. Both minerals are abundant in this granite. The age of 900 ± 9 Ma is considered as a good estimate of the intrusion age of the Absol pluton. The Nd T_{DM} age of this rock (1550 Ma) indicates the existence of Palaeoproterozoic/Archaean material in the source of the Absol pluton. More analysis of zircon cores could perhaps also identify this component.

Eleven zircons have been analyzed from the An Ithnein high-K granite (sample 14-3). The zircon crystals are often elongated and heavily zoned (Fig. 7). Cores are seen but they are also zoned and it is not clear whether they are inherited from older rocks. Seven zircons define a Concordia age at 597 ± 4 Ma (MSWD = 0.04). The other analyses are discordant but form a discordia line giving the same age (601 ± 18 Ma) with a lower intercept at 0 Ma within the large error limits, suggesting Pb loss. Zoned cores have been analyzed and are undistinguishable from the outer parts, demonstrating that all these zircons are magmatic in origin resulting from different stages of the magmatic crystallization. Th/U ratios are medium to high (0.17–0.69), in agreement with a magmatic origin. The age of 597 ± 4 Ma is considered as an excellent estimate of the intrusion age of the An Ithnein pluton. The Nd T_{DM} age of this rock (1190 Ma) indicates the existence of an older material in the source of this pluton but in minor amount probably not present as inherited zircon cores.

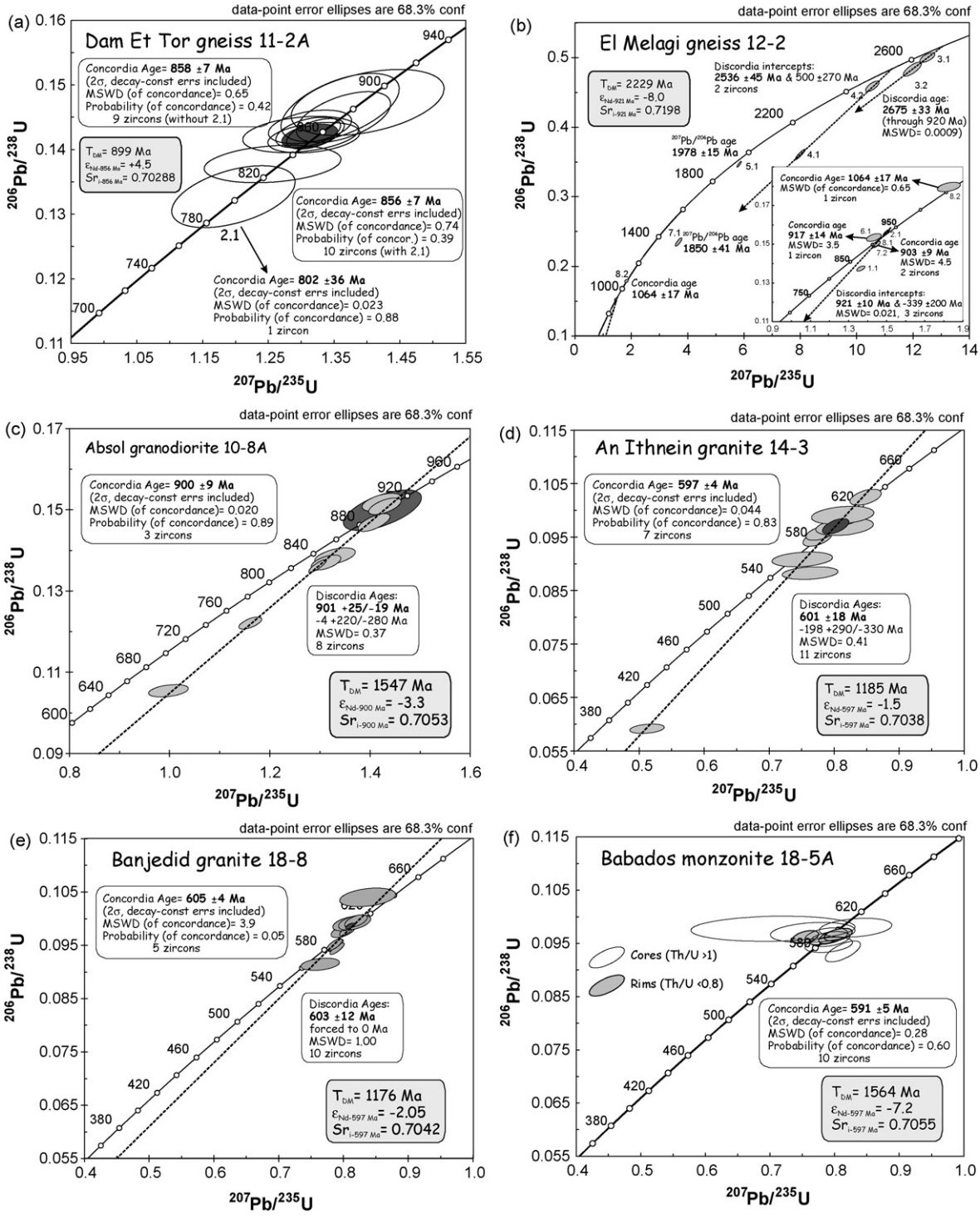

Fig. 7. Concordia diagrams showing the results of zircon age determinations; (a) Dam Et Tor epidote–biotite gneiss, (b) El Melagi muscovite–biotite gneiss, (c) Absol medium-K pluton, (d) An Ithnein high-K pluton, (e) Banjedid high-K pluton and (f) Babados shoshonitic pluton. See text for further explanation.

6.2. Kurmut Series

Eleven zircons from the Dam Et Tor gneiss have been analyzed. The zircon crystals are strongly zoned (Fig. 6); some cores may exist but they are also zoned. Most zircons are stubby but some are very elongated (zircon 2.1; Fig. 6). One analysis (1.1) is not considered due to its large error although it is similar to the other analyses within error limits. Nine concordant zircons define a Concordia age at 858 ± 7 Ma (MSWD = 0.65). All Th/U ratios are high or moderate (0.2–0.5, most between 0.4 and 0.5) in agreement with the magmatic appearance of these zircons. This age of 858 ± 7 Ma can only correspond to the crystallization age of the protolith. The most elongated crystal (2.1) provides a slightly younger concordant age at 802 ± 36 Ma. Due to the large error, it is not clear if this age is meaningful or not. Considering its very elongated habit and its high Th/U ratio (0.44), it is unlikely that this age corresponds to the metamorphic event affecting this sample. We must note that the age calculated with the nine zircons and zircon 2.1

is 856 ± 6 Ma (MSWD = 0.74), which is identical within error limit with the above age. We thus consider that the protolith of the Dam Et Tor epidote–gneiss crystallized at 858 ± 7 Ma and that the metamorphism affected these zircons only slightly or not at all.

6.3. Sabaloka region

In Sabaloka, 10 zircons have been analyzed from the Banjedid high-K granite (sample 18-8). The zircon crystals display often zoned cores and more homogeneous rims. Some zircons are slightly rounded. The three analyzed rims (1.2, 4.2, 5.2) have very low Th/U ratios (0.02–0.03), indicating that these rims are of metamorphic sub-solidus origin. The corresponding zoned cores (1.1, 4.1, 5.1) as well as the other spots, also corresponding to zoned cores, have higher Th/U ratios (0.10–0.17) although still relatively low: this suggests that crystallization of these magmatic zircons occurred contemporaneously with a Th mineral such as monazite. However, the ages of the magmatic cores and of the metamorphic rims are isotopically indistinguishable: five zircons define a Concordia age at 605 ± 4 Ma (MSWD = 3.9). The other analyses are discordant but form a discordia line giving the same age (603 ± 12 Ma, forced to 0 Ma, MSWD = 1.0). This indicates that the Banjedid granite intruded during a high-temperature metamorphism that probably lasted some time after the intrusion, leading to the formation of the rims. The age of 605 ± 4 Ma is considered to correspond to both the intrusion of the granite and to the high-temperature metamorphism that accompanied this major magmatic event. The Nd T_{DM} age of this rock (1180 Ma) indicates the existence of an older material in the source of this pluton. As the latter has not been detected as inherited zircon cores, this older component could also be the ancient lithospheric mantle of the Saharan Metacraton as already suggested by Stern and Dawoud (1991) for Jebel Moya.

Also in Sabaloka, 10 zircons have been analyzed from the Babados shoshonitic monzonite (sample 18-51A). All zircon crystals are elongated to very elongated and display zoned cores with more homogeneous and CL-darker rims. The latter are more or less developed. The cores may be resorbed (crystals 1.1/1.2; 3.1/3.2), nearly not (crystal 4.1/4.2) or not resorbed (crystal 7.1). The rims have in addition to the large development of the prism {1 0 0}, a greater development of the face {1 1 0}, indicating a somewhat cooler medium (Pupin, 1980), suggesting a two-step crystallization story. The analyzed cores have very high Th/U ratios (>1) while the three analyzed rims (1.2, 3.2, 4.2) have lower but still elevated Th/U ratios (0.31–0.75). This suggests that the cores and the rims have crystallized at two distinct stages, probably at two different depths. These magmatic cores and rims are isotopically indistinguishable: all 10 spots are concordant and define a Concordia age at 591 ± 5 Ma (MSWD = 0.28). This age is considered to approximate the age of the intrusion of the Babados monzonite. The Nd T_{DM} age of this rock (1560 Ma) indicates the existence of an older material in the source of this pluton but this does not seem to be present as inherited zircon cores; this is probably due to the high solubility of the zircon in mafic shoshonitic rocks.

7. Sr and Nd isotope geochemistry

Sr and Nd isotopic data of granitoid orthogneisses and plutons are presented in Table 4. In the table Sr and Nd initial ratios of the individual rock suites have been recalculated to the magmatic U–Pb zircon age of the rocks. All the $^{147}Sm/^{144}Nd$ ratios are <0.15 (most are much lower); the Nd T_{DM} model ages can thus be considered as meaningful. Some $^{87}Rb/^{86}Sr$ ratios are very high (up to 15), which prevent a precise calculation of the Sr initial ratios. Sr initial ratios of samples with $^{87}Rb/^{86}Sr > 4$ have been put within brackets in Table 4, for information only; slight weight is given to these values.

7.1. El Melagi muscovite–biotite gneiss

The El Melagi gneiss was metamorphosed at 921 ± 10 Ma. The $\varepsilon_{Nd\,920}$ of −7.1 to −7.9 (Table 4), together with the occurrence of rounded (detrital) and old zircon cores (1.98, 2.54 and 2.68 Ga) indicate that this gneiss was ultimately derived from a pelitic metasediment which had a pre-Neoproterozoic continental source (T_{DM} of 2040–2430 Ma, Table 4). The El Melagi gneiss has very high $^{87}Rb/^{86}Sr$ ratios (10–15), giving unrealistic low initial $^{87}Sr/^{86}Sr$ ratios (SrIR) at 920 Ma ($SrIR_{920}$: 0.6913–0.6886). These meaningless values are most probably the result of the combined effects of high Rb/Sr ratios and a younger metamorphic overprint related to the intrusion of late Pan-African granitoids (cf. the An Ithnein granite dated at 597 ± 4 Ma). This latter event could also be responsible for the development of the thin undated zircon rims in the El Melagi rocks (see above).

7.2. Absol medium-K granite/granodiorite metapluton

The Absol pluton has a concordant zircon age of 900 ± 9 Ma which is interpreted as the age of intrusion and crystallization of the composite pluton. Within the pluton the Sr and Nd isotopic compositions are variable and indicate increasing crustal contamination with increasing differentiation of the magma(s). The tonalitic enclaves are the least contaminated rocks with $\varepsilon_{Nd\,900}$ of −0.3 and $SrIR_{900}$ of 0.7045 (Table 4). Epidote-bearing granodiorites have $\varepsilon_{Nd\,900}$ of −3.3 to −4.3 and $SrIR_{900}$ of 0.7053–0.7055, while biotite granites have $\varepsilon_{Nd\,900}$ of −5.1 but a lower $SrIR_{900}$ of 0.7028 (Fig. 8). The lower SrIR of the highly siliceous granite sample 10-6 (Table 4) is probably due to a higher error on the calculation of the initial ratio, this rock having a higher $^{87}Rb/^{86}Sr$ ratio of 2.2. Sr isotopic data and Nd T_{DM} model ages (1300–1830 Ma) of the Absol pluton both indicate that pre-Neoproterozoic continental crust was progressively incorporated in the magma during its evolution. The nearest surface exposure of such pre-Neoproterozoic crust is in northwestern and western Sudan (Fig. 2). It can therefore be assumed that isotopically similar crust is present at depth below eastern Bayuda Desert (Fig. 8a).

7.3. Dam Et Tor epidote–biotite gneiss

The precursor magma of the Dam Et Tor gneiss crystallized at 858 ± 7 Ma with $\varepsilon_{Nd\,860}$ of 5.7–6.1 and $SrIR_{860}$ of 0.7026–0.7028 (Table 4). These values clearly indicate derivation of the melt from a depleted mantle source, in agreement with the absence of inherited zircon cores and its young Nd T_{DM} model ages of 860–900 Ma (Fig. 9). The gneisses have geochemical characteristics of low- to medium-K calc-alkaline magmas, generated during subduction-related volcanism in a primitive oceanic island arc setting (Küster and Liégeois, 2001). The age of the high-grade metamorphism and deformation of these arc volcanic rocks is not known but should be at 806 ± 19 Ma (Sm–Nd isochron on whole rock; Küster and Liégeois, 2001).

7.4. An Ithnein, Nabati, and Banjedid high-K granite plutons

From the three high-K plutons investigated two were also dated. Greyish porphyritic biotite granite of the An Ithnein pluton from east-central Bayuda Desert yielded a concordant zircon age of 597 ± 4 Ma, while reddish equigranular biotite granite of the Banjedid pluton from Sabaloka yielded a concordant zircon age of

Table 4
Sr and Nd isotope data of granitoid gneisses and plutons from Bayuda Desert and Sabaloka

Sample	Rb	Sr	$^{87}Rb/^{86}Sr$	$^{87}Sr/^{86}Sr \pm 2\sigma$	Sr_i at 920 Ma	Sm	Nd	$^{147}Sm/^{144}Nd$	$^{143}Nd/^{144}Nd \pm 2\sigma$	$^{143}Nd/^{144}Nd$ at 920 Ma	ε_{Nd} 920 Ma	T_{DM} (Ma)
El Melagi muscovite–biotite gneiss												
12-3	259	51	14.96	0.888458 ± 11	(0.691765)	5.46	23.3	0.1418	0.511903 ± 08	0.511047	−7.9	2430
12-2	253	49	15.24	0.891699 ± 11	(0.691342)	3.90	17.3	0.1361	0.511910 ± 09	0.511089	−7.1	2230
12-5b	242	73	9.696	0.816103 ± 13	(0.688607)	1.28	6.34	0.1219	0.511813 ± 09	0.511078	−7.3	2040
Sample	Rb	Sr	$^{87}Rb/^{86}Sr$	$^{87}Sr/^{86}Sr \pm 2\sigma$	Sr_i at 860 Ma	Sm	Nd	$^{147}Sm/^{144}Nd$	$^{143}Nd/^{144}Nd \pm 2\sigma$	$^{143}Nd/^{144}Nd$ at 860 Ma	ε_{Nd} 860 Ma	T_{DM} (Ma)
Dam Et Tor epidote–biotite gneiss												
9-1	9	493	0.0522	0.703456 ± 08	0.702783	0.86	4.41	0.1182	0.512510 ± 11	0.511848	6.1	860
11-2a	27	564	0.1395	0.704277 ± 08	0.702575	1.55	6.81	0.1376	0.512598 ± 12	0.511827	5.7	900
6-3	89	300	0.8588	0.711177 ± 09	0.700699	1.61	10.4	0.0936	0.512348 ± 11	0.511824	5.6	890
Sample	Rb	Sr	$^{87}Rb/^{86}Sr$	$^{87}Sr/^{86}Sr \pm 2\sigma$	Sr_i at 900 Ma	Sm	Nd	$^{147}Sm/^{144}Nd$	$^{143}Nd/^{144}Nd \pm 2\sigma$	$^{143}Nd/^{144}Nd$ at 900 Ma	ε_{Nd} 900 Ma	T_{DM} (Ma)
Absol medium-K pluton												
10-8a	79	314	0.7242	0.714615 ± 07	0.705301	3.73	21.8	0.1033	0.511920 ± 08	0.511310	−3.3	1550
10-7e	84	234	1.036	0.718830 ± 10	0.705500	2.98	14.1	0.1280	0.512013 ± 12	0.511258	−4.3	1830
10-6	123	161	2.221	0.731325 ± 09	0.702754	4.60	23.2	0.1199	0.511923 ± 12	0.511215	−5.1	1820
10-8b	93	366	0.7327	0.713959 ± 11	0.704535	7.27	47.7	0.0922	0.512005 ± 06	0.511461	−0.3	1300
Sample	Rb	Sr	$^{87}Rb/^{86}Sr$	$^{87}Sr/^{86}Sr \pm 2\sigma$	Sr_i at 600 Ma	Sm	Nd	$^{147}Sm/^{144}Nd$	$^{143}Nd/^{144}Nd \pm 2\sigma$	$^{143}Nd/^{144}Nd$ at 600 Ma	ε_{Nd} 600 Ma	T_{DM} (Ma)
Nabati high-K pluton												
15-2	66	167	1.148	0.713023 ± 09	0.703204	6.10	50.9	0.0725	0.512357 ± 15	0.512072	4.1	750
15-1	59	652	0.2617	0.705830 ± 14	0.703590	16.6	99.8	0.1004	0.512264 ± 08	0.511869	0.1	1050
An Ithnein high-K pluton												
14-5	136	323	1.223	0.713539 ± 10	0.703072	2.65	15.4	0.1043	0.512396 ± 11	0.511986	2.4	910
14-7	186	78	6.937	0.760411 ± 08	(0.701052)	4.39	19.8	0.1340	0.512447 ± 07	0.511920	1.1	1140
14-3	164	295	1.612	0.717587 ± 14	0.703794	7.66	43.9	0.1056	0.512203 ± 14	0.511788	−1.5	1190
Banjedid high-K pluton												
18-8	94	391	0.696	0.710154 ± 10	0.704200	2.60	16.3	0.0965	0.512139 ± 13	0.511760	−2.1	1180
17-4b	159	353	1.304	0.714034 ± 09	0.702874	1.00	10.8	0.0556	0.511845 ± 09	0.511627	−4.7	1160
Banjedid shoshonitic dykes												
17-4f	299	249	3.484	0.733624 ± 09	0.703815	22.2	144	0.0936	0.511919 ± 07	0.511551	−6.1	1430
18-1b	268	178	4. 373	0.744304 ± 09	(0.706890)	27.5	218	0.0760	0.511741 ± 11	0.511442	−8.3	1440
18-1c	292	141	6.022	0.757608 ± 09	(0.706079)	13.0	112	0.0701	0.511833 ± 11	0.511557	−6.0	1290
Babados shoshonitic pluton												
18-5a	257	256	2.912	0.730435 ± 12	0.705522	26.3	155	0.1030	0.511905 ± 10	0.511500	−7.1	1560
Suleik shoshonitic pluton												
18-7	286	140	5.941	0.757669 ± 09	(0.706838)	11.5	75.4	0.0924	0.511995 ± 09	0.511632	−4.6	1320
18-6b	187	185	2.932	0.730458 ± 09	0.705374	4.78	43.0	0.0673	0.511853 ± 10	0.511589	−5.4	1240

Sr and Nd initial ratios of the individual granitoid occurrences have been recalculated to their magmatic U–Pb zircon age. Samples from high-K and shoshonitic plutons were however all recalculated to 600 Ma for comparative purposes. Nd T_{DM} ages were calculated following Nelson and De Paolo (1985).

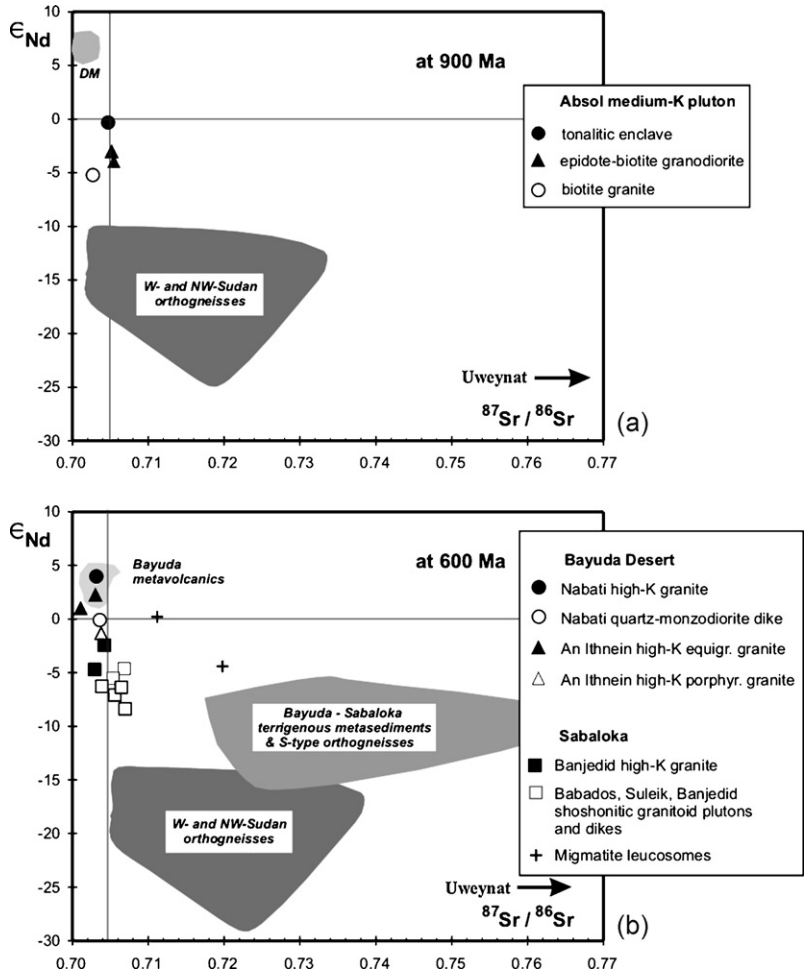

Fig. 8. Plot of Sr initial ratios vs. ε_{Nd} values of (a) Absol medium-K pluton recalculated to 900 Ma and (b) post-collisional high-K and shoshonitic plutons and dikes recalculated to 600 Ma. Data for migmatite leucosomes from Sabaloka are unpublished data of first author. Isotopic composition of basement rocks from western and northwestern Sudan are from Harms et al. (1990) and Davidson and Wilson (1989); those of metavolcanics, terrigenous metasediments and S-type orthogneisses from Bayuda Desert and Sabaloka are from Küster and Liégeois (2001).

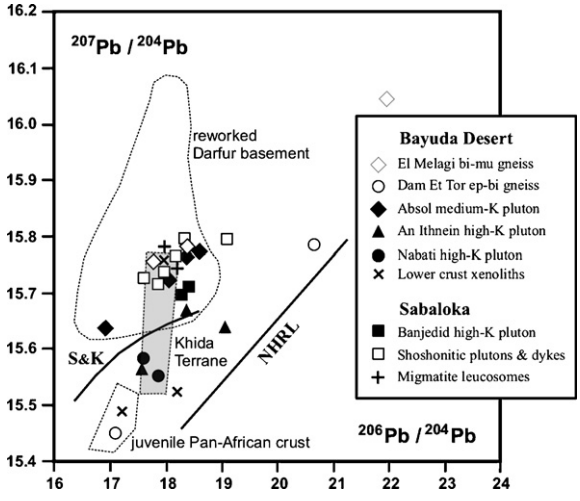

Fig. 9. Plot of initial $^{207}Pb/^{204}Pb$ vs. $^{206}Pb/^{204}Pb$ isotope composition of granitoid gneisses and post-collisional granites from Bayuda Desert and Sabaloka. Data sources: Bayuda Desert lower crust xenoliths and Sabaloka migmatite leucosomes (F. Lucassen, unpublished data); Darfur metamorphic and plutonic rocks (Davidson and Wilson, 1989; F. Lucassen, unpublished data); Khida Terrane (Stoeser and Frost, 2006); Pan-African juvenile crust (Stern and Kröner, 1993; Zimmer et al., 1995; Stern and Abdelsalam, 1998). S&K: crustal lead evolution; Stacey and Kramers, 1975; NHRL: Northern Hemisphere Reference Line; Hart, 1984.

605 ± 4 Ma. Sr and Nd isotopic data of all high-K rocks were recalculated to 600 Ma for comparative purposes. As a group the high-K plutons (Nabati, An Ithnein, Banjedid) have low and rather homogeneous $SrIR_{600}$ (0.7029–0.7042), except one high-silica sample from An Ithnein pluton (14-7) which has a lower value of 0.7011 (Table 1). Due to a high error linked to its high $^{87}Rb/^{86}Sr$ ratio (Table 1), this low value is not considered to be meaningful. On the other hand, the high-K granites display heterogeneous $\varepsilon_{Nd\,600}$ values between +4.1 and −4.7 and Nd T_{DM} model ages between 750 and 1190 Ma (Table 1, Figs. 8b and 9a). The rather homogenous Sr isotopic composition of the magmas (0.7029–0.7042) compared to the variability of their ε_{Nd} (+4 to −5) suggests that the subcontemporaneous metamorphic overprint depicted by the zircon dating has been able to homogenize the Sr isotope but not the Nd isotope composition, pointing to a heterogeneous source for these high-K calc-alkaline granites or, more probably, to a juvenile source variably contaminated by an older crust.

The Nabati and An Ithnein plutons from Bayuda Desert display Sr and Nd isotopic compositions ($SrIR_{600}$: 0.7030–0.7038; $\varepsilon_{Nd\,600}$: +4 to +0.1) close to the high-grade metavolcanic basement of the Kurmut Series in eastern Bayuda Desert (Fig. 8b), with the exception of the An Ithnein porphyritic granite sample 14-3 ($\varepsilon_{Nd\,600}$ of −1.7). This suggests that the source of these granitoids could be the Kurmut lower crust or lithospheric mantle. Their potassic character is typical of the remelting of a lithospheric mantle meta-

somatized during a former subduction or of the correlated lower crust (Liégeois et al., 1998). The assimilation of the equivalent of the Rahaba Series at depth is possible but only in minor amounts. The Nabati quartz–monzodiorite dyke emplaced within the Kurmut Series has isotopic compositions ($\varepsilon_{Nd\,600}$ of +0.1, $SrIR_{600}$ of 0.7036) within the range of the high-K plutons from the Rahaba Series (central Bayuda) and Sabaloka. Compared to its host Nabati pluton, the $\varepsilon_{Nd\,600}$ value of the dyke is however less radiogenic (Fig. 8b). By nature, the dyke is younger than its hosting high-K pluton and we consider the quartz–monzodiorite as a fractionated mantle melt. Its isotopic composition derived either from a slightly enriched mantle source (CLM) or by limited crustal contamination (pre-Neoproterozoic component) of a depleted mantle melt.

The Banjedid high-K pluton from Sabaloka has $SrIR_{600}$ (0.7033–0.7044) similar to the Bayuda high-K plutons, but displays even more negative $\varepsilon_{Nd\,600}$ values (−2.1 to −4.7). This suggests derivation of the Banjedid granite from isotopically heterogeneous lower crustal protoliths. We infer the presence of a juvenile Neoproterozoic component and, taking into account the low Sr initial ratios, an Rb-poor pre-Neoproterozoic component (Figs. 8b and 9). The middle to upper crust which is presently exposed at the surface at Sabaloka and Bayuda is unlikely to be the source or contaminant of the Banjedid high-K granite, since it has much higher $SrIR_{600}$ (Fig. 8b). Migmatitic leucosomes which were investigated along with the granite plutons at Sabaloka are clearly derived from this crust and isotopically deviate from the Banjedid pluton (Fig. 8b). Isotope data from the leucosomes show that the middle to upper crust at Sabaloka/Bayuda is heterogeneous and probably formed from a mixture of juvenile Neoproterozoic metavolcanic gneisses and Neoproterozoic terrigeneous metasediments (Fig. 8b). The latter were largely derived from pre-Neoproterozoic continental sources.

7.5. Babados, Suleik, and Banjedid shoshonitic granite plutons and dykes

Out of the shoshonitic granitoids at Sabaloka, the Babados pluton was dated and yielded a concordant zircon age of 591 ± 5 Ma. This age can be assumed as the emplacement and crystallization age of all shoshonitic granitoids (plutons and dykes) in the area and are thus ca. 10 Ma younger that the high-K granites. Sr and Nd isotopic data of all shoshonitic granitoids were recalculated to 600 Ma to compare them with the high-K granites.

Isotopically the shoshonitic granitoids cluster together as a distinct group in the ε_{Ndt}–$^{87}Sr/^{86}Sr$ diagram (Fig. 8b), having values between −4.6 to −8.3 and 0.7038 to 0.7069, respectively. The isotopic data suggest that the shoshonitic melts derived either from the lithospheric mantle (to account for their very high K_2O content; Liégeois et al., 1998) variably contaminated by crustal material in the lower crust, or from a heterogeneous mafic crustal source comprising both juvenile and old components.

8. Pb isotope geochemistry

Measured and initial Pb isotope ratios vary widely (Fig. 9; Table 5), but most samples are restricted to initial $^{206}Pb/^{204}Pb$ ratios of ~17.2 to 19.4. The $^{207}Pb/^{204}Pb$ ratios show systematic differences if compared with the evolution of average crustal Pb isotope composition (Stacey and Kramers, 1975). All samples from the Sabaloka localities as well as the samples from the Rahaba–Absol Series of

Table 5
Pb isotopic composition of granitoid gneisses and granitic plutons from Bayuda Desert and Sabaloka

Sample	Pb (ppm)	U (ppm)	Th (ppm)	U/Pb	Th/U	μ	ω	$^{206}Pb/^{204}Pb$	$(^{206}Pb/^{204}Pb)_i$	$^{207}Pb/^{204}Pb$	$(^{207}Pb/^{204}Pb)_i$	$^{208}Pb/^{204}Pb$	$(^{208}Pb/^{204}Pb)_i$
El Melagi muscovite–biotite gneiss 921 Ma													
12-3	23.9	5.59	12.1	0.23	2.16	15.5	34.6	20.58	18.20	15.95	15.78	39.02	37.40
12-2	20.2	3.60	8.57	0.18	2.38	12.4	30.5	24.14	22.24	16.20	16.07	38.91	37.49
12-5b	30.0	1.27	3.76	0.04	2.97	2.7	8.3	18.84	18.43	15.82	15.79	38.07	37.68
Dam Et Tor epidote–biotite gneiss 858 Ma													
11-2a	4.47	0.53	0.83	0.12	1.57	7.4	12.0	18.29	17.24	15.53	15.46	37.42	36.91
6-3	13.5	3.46	11.6	0.26	3.35	18.1	62.7	23.62	21.05	15.99	15.81	40.91	38.21
Absol medium-K pluton 900 Ma													
10-7E	22.9	3.57	6.77	0.16	1.90	10.1	19.8	19.77	18.26	15.86	15.75	38.45	37.55
10-8A	17.6	3.66	8.61	0.21	2.36	13.4	32.7	19.23	17.22	15.80	15.66	38.93	37.44
10-8B	16.1	4.08	8.93	0.25	2.19	17.1	38.7	21.48	18.92	15.98	15.81	39.52	37.76
10-6	25.7	2.31	11.5	0.09	5.00	5.8	30.2	19.34	18.47	15.84	15.78	39.04	37.67
An Ithnein high-K pluton 597 Ma													
14-5	21.3	2.48	13.1	0.12	5.29	7.6	41.3	19.91	19.18	15.69	15.64	38.64	37.40
14-7	29.5	15.0	20.4	0.51	1.36	34.0	47.6	21.35	18.06	15.79	15.59	38.91	37.48
14-3	22.2	6.95	26.0	0.31	3.71	20.9	80.1	20.70	18.67	15.81	15.69	39.70	37.30
Nabati high-K pluton (597 Ma)													
15-1	14.4	3.31	12.5	0.23	3.78	15.0	58.4	19.27	17.82	15.68	15.60	39.27	37.52
15-2	13.8	2.33	8.40	0.17	3.61	10.8	40.3	19.07	18.02	15.63	15.56	38.52	37.31
Banjedid high-K pluton 605 Ma													
18-8	34.1	2.04	7.52	0.06	3.69	3.8	14.5	18.71	18.34	15.73	15.70	38.45	38.02
17-4b	35.8	0.98	17.6	0.03	17.9	1.8	32.7	18.57	18.40	15.73	15.71	39.22	38.24
Banjedid shoshonitic dykes (591 Ma)													
17-4f	37.2	1.19	43.8	0.03	36.9	2.1	80.8	18.29	18.08	15.75	15.74	41.69	39.27
18-1B	36.0	4.52	147	0.13	32.6	8.6	289	18.58	17.74	15.79	15.74	43.65	35.01
18-1c	42.8	2.24	97.2	0.05	43.5	3.5	157	18.60	18.27	15.79	15.77	41.72	37.03
Babados shoshonitic pluton 591 Ma													
18-5A	28.9	2.06	46.9	0.07	22.7	4.7	111	18.38	17.93	15.75	15.72	41.13	37.86
Suleik shoshonitic pluton (591 Ma)													
18-7	38.8	12.2	59.6	0.31	4.88	22.0	111	21.51	19.41	15.94	15.81	42.36	39.08
18-6b	30.3	2.10	19.4	0.07	9.26	4.5	43.5	18.83	18.39	15.82	15.80	40.38	39.09

north-central Bayuda Desert (El Melagi gneiss, Absol pluton) show distinctly higher $^{207}Pb/^{204}Pb$ ratios than average crustal Pb. The samples from the Kurmut Series in eastern Bayuda Desert (Dam Et Tor gneiss, Nabati pluton) have lower $^{207}Pb/^{204}Pb$ values at a similar range of $^{206}Pb/^{204}Pb$ ratios (Fig. 9). Th and U element concentrations of the samples are uncorrelated as are the thorogenic $^{208}Pb/^{204}Pb$ and uranogenic $^{206}Pb/^{204}Pb$ and $^{207}Pb/^{204}Pb$ ratios. Also, no correlation exists between the μ or w values and the calculated Pb initial ratios, which suggests no major recent U mobility; we thus consider that these calculated Pb initial ratios correspond to the true initial Pb initial ratios.

The initial high $^{207}Pb/^{204}Pb$ ratios of rocks from Sabaloka and north-central Bayuda Desert compare to high $^{207}Pb/^{204}Pb$ rocks in the Darfur region of western Sudan (Davidson and Wilson, 1989; unpublished data, F. Lucassen) and the pre Pan-African Khida fragment of the Arabian Shield (Stoeser and Frost, 2006). Both are considered as typical Pb isotope signatures of (reworked) cratonic crust (Fig. 9) and indicate that pre-Neoproterozoic crust is present at Sabaloka and in the north-central part of Bayuda Desert. Samples from the Kurmut Series in the eastern part of Bayuda Desert are similar to juvenile Pan-African material (Fig. 9). This suggests that the eastern part of Bayuda Desert is composed of juvenile Neoproterozoic crust with only minor involvement of older components and is consistent with the data of Bailo et al. (2003) for the region to the NE of Bayuda Desert. The variable Pb isotopic composition and the mixed age of the Bayuda Desert crust is also evident from Pb isotopes of lower crustal xenoliths from the Main Volcanic Field of Central Bayuda Desert (unpublished data of F. Lucassen; Fig. 9). Two of these mafic garnet granulites have juvenile Neoproterozoic Pb compositions while a third granulite is comparable to reworked older crust.

9. Discussion: geodynamics and crustal structure at the eastern edge of the Saharan Metacraton

Our study was undertaken to get more insight into the Pan-African (850–550 Ma) magmatic and metamorphic history of the eastern boundary region of the Saharan Metacraton for which a Palaeoproterozoic and Archaean evolution is documented further to the west. U–Pb geochronology on zircons showed however the unexpected existence of a 920–900 Ma pre-Pan-African tectono-magmatic/metamorphic phase. The Pan-African (s.s.) orogenic climax occurred at ca. 600 Ma, corresponding to the formation of Greater Gondwana or Pannotia (Stern, 2008). However, orogenic cycles most often begin by accretion of oceanic arcs on passive continental margins prior to major intercontinental collisions. As specified in the introduction, we thus consider the amalgamation of various oceanic arcs in the ANS (850–650 Ma) as part of the Pan-African (s.l.) orogenic cycle (850–550 Ma). Such early Pan-African events are also common at the eastern boundary of the Saharan Metacraton. To the NW of Bayuda Desert along the Atmur-Delgo Suture, subduction-derived low-grade rocks of ANS derivation were thrust southeastwards during nappe emplacement at 760–700 Ma (Schandelmeier et al., 1994a,b; Harms et al., 1994; Abdelsalam et al., 1995, 1998; Abdelsalam and Stern, 1996). The Dam Et Tor sequence studied here can easily be grouped with this early Pan-African arc accretion. These 858 ± 7 Ma (U–Pb zircon age) old juvenile oceanic rocks (T_{DM}: 860–900 Ma) were probably accreted at 806 ± 19 Ma (Sm–Nd isochron; Küster and Liégeois, 2001). The Dam Et Tor sequence actually corresponds to the oldest dates known from the ANS (~850 Ma; Stern, 1994; Avigad et al., 2007), but can still be considered as part of the Pan-African orogenic cycle. By contrast, the continental-derived older El Melagi gneiss (921 ± 10 Ma U–Pb zircon age; T_{DM}: 2040–2430 Ma) and the Absol metagranite (900 ± 9 Ma U–Pb zircon age; T_{DM}: 1550–1830 Ma) cannot be integrated within this Pan-African oceanic accretionary evolution. They constitute an older pre-Pan-African event. This is the reason why we suggest considering an independent "Bayudian" episode rather than a "very early Pan-African" phase. This Bayudian event concerns the eastern boundary of the Saharan Metacraton. It occurred during the Tonian period (1000–850 Ma; Plumb, 1991) of the early Neoproterozoic, a period which otherwise on Earth was tectono-magmatically relatively quiescent (Stern, 2008).

9.1. The early Neoproterozoic (Tonian) Bayudian episode in north-central Bayuda Desert

The Bayudian episode is documented by 921 ± 10 Ma amphibolite-facies metamorphism (El Melagi peraluminous gneiss) and 900 ± 9 Ma granitoid magmatism of the medium-K Absol pluton. Earlier Rb–Sr whole rock errorchrons on gneisses from Bayuda Desert have given doubtful ages of 874 Ma (Meinhold, 1979) and 898 Ma (Ries et al., 1985), leading however already these authors to suggest a pre-Pan-African origin for the Bayuda Desert basement or part of it. The zircon cores dated in the El Melagi gneiss indicate that the source of the metasediments comprise principally Archaean (2.67 and 2.53 Ga) and Palaeoproterozoic (1.98 and 1.85 Ga) lithologies, ages that are known in the Uweynat inlier to the NW (Klerkx and Deutsch, 1977). The source of the El Melagi sediments can thus be ascribed to the Saharan Metacraton. Their depositional age can be bracketed between 920 Ma (the age of metamorphism) and probably 1064 ± 17 Ma, the age of the youngest concordant zircon core in the gneiss (Fig. 7b). This latter "Grenvillian" age is presently supported by only one El Melagi zircon and certainly needs further confirmation. However, 1.0–1.1 Ga Grenvillian ages have also been obtained in detrital zircons from Lower Palaeozoic sandstones of northern Ethiopia (Avigad et al., 2007) and Israel (Avigad et al., 2003), suggesting that late Mesoproterozoic source rocks were likely present in a wider region.

The El Melagi metasediments were metamorposed at ca. 920 Ma and followed by a 900 ± 9 Ma magmatic event represented by the Absol pluton. The amphibolite-facies metamorphism and thrust deformation of the El Melagi gneiss, the medium-K geochemistry and the predominantly crustal sources of the Absol pluton and the absence of any typical active margin lithologies suggest that the 920–900 Ma Bayudian event was an orogenic event, the Absol pluton being emplaced in a post-collisional setting. An alternate hypothesis that would relate the Bayudian event to rift genesis such as that proposed for the Rahib and Umm Badr Belts (Schandelmeier et al., 1990) does not match the above constraints. With only the current data available, it is not possible to further precise the nature of this Bayudian orogenic event. However, it could be a regionally significant event as similar ages are cited by De Wit et al. (2005) in southern and eastern Chad and a set of detrital zircons have been dated in the 0.89–0.93 Ga age range in northern Ethiopia (Avigad et al., 2007) and around 0.9 Ga in Israel (Avigad et al., 2003). In turn, this means that the unknown source of these detrital zircons (Avigad et al., 2003; 2007) could be the Bayudian segment from the Saharan Metacraton. More strikingly, granulite-facies metasedimentary gneisses at Sabaloka contain substantial amounts of rounded Bayudian aged (900–976 Ma) zircons (Kröner et al., 1987). This probably indicates that the Sabaloka region was collecting the detritus of the exhumed and eroding Bayudian segment during the early Pan-African. The Bayudian segment could correspond to the Zalingei folded zone (Vail, 1976, 1989). This zone is characterized by NE-trending foliations and stretches from the Bayuda and Nubian Deserts west of the Nile through northern Kordofan and Wadi Howar up to the J. Marra/Darfur Dome in western

Sudan (see Fig. 2). It may also continue into eastern Chad, towards the ~900 Ma granitoids reported there (De Wit et al., 2005). More data are however needed for assessing the correlation between the Zalingei folded zone and the Bayudian event depicted in this study. On a global scale the Bayudian event has an age comparable to the end of the Sveconorwegian orogeny in SW Scandinavia where metamorphic episodes have been dated at ca. 930 Ma and ca. 913 Ma and leucosome formation at 892 ± 4 Ma (U–Pb zircon ages, Lundmark and Corfu, 2008).

9.2. Early Pan-African juvenile magmatic episode in eastern Bayuda Desert

Zircons from the Dam Et Tor medium-K epidote–biotite orthogneiss yielded a magmatic formation age of 858 ± 7 Ma with only slightly older Nd T_{DM} model ages (860–900 Ma). The magmatic precursor of the gneiss is interpreted as a rhyodacitic volcanic or subvolcanic rock which was formed at a rather primitive intra-oceanic arc system. Sr, Nd and Pb isotope characteristics indicate juvenile sources for this subduction-related magmatism with no indication of the involvement of older pre-Neoproterozoic crust. This means that the arc-derived Kurmut Series, to which the Dam Et Tor assemblage belongs, formed far away from any continent, distant also from the Saharan Metacraton and its Bayudian margin. Metamorphism and deformation of these arc volcanic rocks occurred most probably at 806 ± 19 Ma, the age of a Sm–Nd WR isochron on arc-derived rocks from eastern Bayuda Desert (Küster and Liégeois, 2001). The isochron involves mainly amphibolitic rocks but also epidote–biotite gneisses including the sample 11-2a which was used for zircon geochronology. This 806 Ma event is considered as corresponding to the accretion of the Kurmut arc towards the Saharan Metacraton.

9.3. Existence of two distinct terranes in the basement of Bayuda Desert

The continental pre-Pan-African derivation of the El Melagi gneiss and Absol pluton is strongly indicated by old inherited zircons, pre-Neoproterozoic Nd T_{DM} model ages and radiogenic common Pb isotope signatures. El Melagi gneiss and Absol pluton are part of the Rahaba and Absol Series of the Bayuda Desert (Barth and Meinhold, 1979) and we propose here to call the area composed of these two Series the *Rahaba–Absol Terrane*. This terrane belongs to the Saharan Metacraton and, for the time being, will be considered a sub-terrane of the previously defined and broader Bayuda Terrane (Abdelsalam and Stern, 1996). The continental derivation of the Rahaba–Absol Terrane is strikingly different from the juvenile oceanic nature of the Kurmut Series in eastern Bayuda Desert. We thus propose to call the remnant of this early Pan-African island arc the *Kurmut Terrane*. This terrane belongs to the ANS, its accretion actually marks the beginning of a period of arc amalgamation further to the east. The Kurmut Terrane could be considered a sub-terrane of the composite Gabgaba/Gebeit Terrane (ANS) but only if the Keraf Zone is included in the latter.

The terrane discrimination implies that the correlation between the Absol Series and the Dam Et Tor sequence based on lithostratigraphic correlations (Vail, 1971, 1988) or on the geochemistry of amphibolites (Küster and Liégeois, 2001) cannot anymore be envisaged. This is confirmed by our field investigation: we found abundant biotite and epidote–biotite gneisses (including the dated sample 11-2A) at Dam Et Tor whose predominance is typical of the Kurmut Series (Barth and Meinhold, 1979), but is absent in the Absol Series. This also implies that the boundary between the Absol and Kurmut Series, i.e. the boundary between the Rahaba–Absol and Kurmut terranes, lies 15 km further to the north than previously considered (Barth and Meinhold, 1979) and thus approximately coincides with the northern limit of the Dam Et Tor Fold/Thrust Belt (Fig. 3). The terrane boundary between the Rahaba–Absol and Kurmut terranes corresponds, at the surface, to the boundary between the Saharan Metacraton and the Arabian–Nubian Shield. The juvenile character of the Nabati pluton (Nd T_{DM} of 750 and 1050 Ma) emplaced within the Kurmut Terrane suggests that the Saharan Metacraton is rapidly disappearing at depth to the east and confirms the suggestion of Abdelsalam and Stern (1996) that the Keraf shear zone marks its eastern lithospheric boundary.

9.4. Late Pan-African magmatic episode in Bayuda Desert

The first event recorded by both the Rahaba–Absol Terrane and the Kurmut Terrane following accretion of the latter at ca. 800 Ma is the intrusion of post-collisional granites during the Pan-African climax (~600 Ma). In the Rahaba–Absol Terrane the emplacement of the An Ithnein type granitoids at 597 ± 4 Ma was accompanied by high-temperature metamorphism. This metamorphism is likely responsible for the development of epidote and garnet in the Absol pluton and probably for the thin outer rims in zircons from El Melagi gneiss. Post-collisional granitoids within the Kurmut Terrane have not been dated by zircon geochronology: however, a K/Ar biotite age of 584 Ma (Meinhold, 1979) and a Rb/Sr WR errorchron age of 600 ± 19 Ma (MSWD = 6.23) performed during this study confirms that granitoid emplacement in the Kurmut Terrane was late Pan-African in age. The late Pan-African magmatic events are contemporaneous with transpressive functioning of the Keraf shear zone (Abdelsalam and Stern, 1996), which is typical of the post-collisional period (Liégeois et al., 1998). As the plutons are present in both the Bayudian Rahaba–Absol Terrane and the juvenile Pan-African Kurmut Terrane, we can suspect that the granitoid magmas pursued the Keraf shear zones from their source to the surface dispersing themselves in the brittle crust in a wider area (Acef et al., 2003; Liégeois et al., 2003). The high-K plutons from Bayuda Desert (Nabati, An Ithnein) have isotopic compositions ($SrIR_{600}$ ~0.7035, $\varepsilon_{Nd\ 600}$ = 0 to +4, $^{207}Pb/^{204}Pb < 15.6$) characteristic of a juvenile Neoproterozoic crust or of the mantle. Consequently, such a protolith must constitute large parts of the lower crust in eastern Bayuda Desert (Kurmut Terrane). A role can be ascribed to the SmC crust by the isotopic characteristics of the porphyritic facies of the An Ithnein pluton (Table 4, Figs.8b and 9).

9.5. The rheological behaviour of the Bayudian segment during the Pan-African orogenic cycle

Two additional observations are striking when considering the above data: (1) in the Rahaba–Absol Terrane there is no record of tectono-magmatic activity during the 860–620 Ma period (i.e. almost the entire Pan-African orogenic cycle except the end) and (2) in the Kurmut Terrane there is also no trace of tectono-magmatic activity between roughly 750–650 Ma. The entire Bayuda Desert has thus experienced an interval of more than 100 Ma when tectonic and magmatic activity apparently ceased. This can be integrated in a model with four stages where the eastern boundary of the SmC was always located on the subducting plate: (1) the SmC eastern boundary collided with an unknown continent at 920–900 Ma giving rise to the Bayudian segment; this unknown continent would have escaped through transpression movements in a similar model as that invoked for the Laramian orogeny in western America (Maxson and Tikoff, 1996); (2) collided with the ca. 850 Ma old Kurmut arc at 800 Ma, the latter being accreted towards the SmC; (3) a quiescent period between 800 and 650 Ma due to the rigid characteristics of the Saharan Metacraton (a metacraton

preserves most of the rigidity of a craton) and to the migration of the arc accretion elsewhere in the ANS; and (4) the SmC eastern boundary with its Kurmut superstructure was involved in the huge Keraf transpression event (640–580 Ma, Abdelsalam et al., 1998), inducing a HT metamorphism and the intrusion of post-collisional granitoids, corresponding to the formation of Greater Gondwana or Pannotia (Stern, 2008).

9.6. Late Pan-African magmatic episode at Sabaloka

Late Pan-African post-collisional granitoid magmatism occurred also in Sabaloka region. High-K calc-alkaline biotite granite plutons were emplaced at 605 ± 4 Ma (Banjedid pluton) and are slightly older than the shoshonitic Babados pluton emplaced at 591 ± 5 Ma. The younger age of the shoshonitic granitoids is in line with crosscutting relationships observed in the Banjedid pluton. Similar granitoids are of widespread occurrence elsewhere in the region (Harms et al., 1990; Pudlo and Franz, 1994; Küster and Harms, 1998). This post-collisional granitoid magmatism is probably also coeval with HT metamorphism. The Sabaloka granites display zircon rims with low Th/U ratios suggesting that they crystallized in sub-solidus conditions, comparable to a metamorphic event. However, as the age of these zircons rims are analytically identical to the cores, we can conclude that a regional high heat flow was responsible for both the magmatism and the HT metamorphism, as typically observed in post-collisional settings (Liégeois et al., 1998). Cooling ages of the two post-collisional granitoid suites from Sabaloka can be inferred from Rb–Sr whole rock dating (carried out during this work but yielding only errorchrons with MSWD > 2) and are around 585–575 Ma.

The Banjedid high-K pluton and the shoshonitic plutons and dykes from Sabaloka have Pb isotopic compositions ($^{207}Pb/^{204}Pb > 15.7$) characteristic of reworked older crust (Fig. 9). However, Sr and Nd isotopic compositions ($SrIR_{600} = 0.703$ to 0.707, $\varepsilon_{Nd\ 600} = -2$ to -8) are intermediate between a juvenile Neoproterozoic crust and an older Rb-poor pre-Neoproterozoic crust (Fig. 10), but different from the crust presently exposed at surface which has a much higher $SrIR_{600}$ (>0.720). The Banjedid high-K granite probably has been derived from a crustal mixture of both components, while the mantle-derived shoshonitic magma digested substantial amounts of pre-Neoproterozoic crust during crystallization. Pre-Pan-African rocks with such isotopic compositions must therefore be present at depth and confirms that Sabaloka is part of the Saharan Metacraton. The crust from the Sabaloka region may be isotopically comparable with the Rahaba–Absol Terrane of Bayuda Desert. However, there are indications that the Neoproterozoic geodynamical evolution of the Sabaloka region is different from the latter. Although grey biotite gneisses constitute the commonest rock type, the Sabaloka basement is characterized by widespread migmatisation and a relic granulite facies metamorphism (Almond, 1980), dated at ~700 Ma (Kröner et al., 1987). Although these zircon ages are somewhat equivocal and granulite facies metamorphism could be as young as 620 Ma (U–Pb monazite age, V. Schenk, personal communication), the age of high-grade metamorphism at Sabaloka is Pan-African and not Bayudian (920 Ma) as in the Rahaba–Absol Terrane. Furthermore, the granulite facies metasedimentary gneisses at Sabaloka contain rounded probably detrital zircons with ages as young as 900 Ma (Kröner et al., 1987) and apparently have a younger depositional age than the El Melagi gneiss. The Rahaba–Absol Terrane could have actually been the source of the early Pan-African Sabaloka metasediments. We therefore propose the name *Sabaloka Terrane* for the crust of the Sabaloka region, highlighting a different geodynamical evolution of this part of the SmC during the Pan-African orogenic cycle.

10. Conclusions

The geochronological and isotopic study of granitoid rocks from the eastern boundary of the Saharan Metacraton indicate that the Bayuda Desert and Sabaloka region records orogenic events starting in the early Neoproterozoic (920–900 Ma: Bayudian event) and ending during late Pan-African times (ca. 600–580 Ma).

(1) Peraluminous El Melagi granitoid gneisses were metamorphosed at 921 Ma probably in a syn-collisional setting. The El Melagi zircons contain detrital cores with ages between 1060 and 2675 Ma, indicating that the pelitic sediment from which the gneiss derived was shed from Proterozoic and late Archaean sources and probably deposited in a late Mesoproterozoic (<1060 Ma) to early Neoproterozoic (>920 Ma) basin.
(2) The medium-K Absol granite–granodiorite pluton in northeastern Bayuda Desert was discordantly emplaced at 900 Ma into high-grade metamorphic schists and amphibolites of the Absol Series. The Absol pluton was only slightly affected by later Pan-African metamorphism (growth of garnet and epidote), but was not tectonically deformed.
(3) Sr, Nd and Pb isotopic data indicate that the El Melagi gneiss and the post-collisional Absol pluton were derived from, or substantially contaminated with, pre-Neoproterozoic crust. Together with the Absol metavolcanosedimentary Series the Bayudian granitoids therefore define the Bayudian Rahaba–Absol Terrane belonging to the Saharan Metacraton.
(4) The magmatic precursor of the medium-K Dam Et Tor gneiss in eastern Bayuda Desert crystallized at 858 Ma. The magma was generated from a depleted mantle source during early Pan-African oceanic arc magmatism. The Dam Et Tor gneiss is considered to be a member of the Pan-African Kurmut metavolcanosedimentary Series and was metamorphosed during the Pan-African cycle, probably as early as 806 Ma (Sm–Nd WR isochron).
(5) The Dam Et Tor gneiss and its hosting Kurmut Series are part of the Arabian–Nubian Shield (Keraf Zone) and constitute the Kurmut Terrane of eastern Bayuda Desert. They are in tectonic contact with the Rahaba–Absol Terrane along the Abu Hamed and Dam Et Tor fault/thrust belts. In the Bayuda Desert these thrust belts constitute the boundary between the ANS and the Saharan Metacraton.
(6) Post-collisional granitoid magmatism occurred between 605 and 591 Ma and yielded high-K granite plutons in Bayuda Desert as well as high-K and shoshonitic granite plutons in Sabaloka. Emplacement of the plutons was contemporaneous with late Pan-African HT metamorphism related to post-collisional crustal extension and uplift.
(7) Sr, Nd and Pb isotopic data indicate that the high-K granites from Bayuda Desert (Nabati and An Ithnein plutons) derived from juvenile Neoproterozoic crust or from the mantle. The An Ithnein pluton was emplaced in the Bayudian Rahaba–Absol Terrane and experienced minor interaction with the pre-Neoproterozoic crust.
(8) Sr, Nd and Pb isotopic data indicate that the high-K and shoshonitic granites from Sabaloka (Banjedid, Babados and Suleik plutons) derived from, or were strongly contaminated with pre-Neoproterozoic crust. Contrary to the Rahaba–Absol Terrane of Bayuda Desert this crust experienced Pan-African high-grade metamorphism (Kröner et al., 1987), and Sabaloka thus constitutes another distinct terrane within the Saharan Metacraton.
(9) Pre-Neoproterozoic crust of the Saharan Metacraton further to the west of the study area (i.e. Zalingei folded zone in central and western Sudan) is in structural continuity with the

Bayuda Desert basement. The Zalingei zone could therefore also comprise areas of Bayudian ancestry, largely unaffected by Pan-African deformation. Precise age determinations are however needed to verify this assumption.

Acknowledgements

We would like to thank Ahmed S. Dawoud for guidance and assistance in the field. The first author acknowledges financial support of Deutsche Forschungsgemeinschaft (DFG) by grant Ku-887/3-1 and F. Lucassen by DFG grant FR 557/20-1. Bob Stern is thanked for his constructive comments that enhanced the clarity and the impact of this paper.

References

Abdelsalam, M.G., Stern, R.J., 1996. Sutures and shear zones in the Arabian–Nubian Shield. J. Afr. Earth Sci. 23, 289–310.
Abdelsalam, M.G., Stern, R., Schandelmeier, J., Sultan, H.M., 1995. Deformational history of the Keraf zone in northeast Sudan, revealed by Shuttle Imaging Radar. J. Geol. 103, 475–491.
Abdelsalam, M.G., Stern, R.J., Copeland, P., El Faki, E.M., El Hur, B., Ibrahim, F.M., 1998. The Neoproterozoic Keraf Suture in NE Sudan: sinistral transpression along the eastern margin of West Gondwana. J. Geol. 106, 133–147.
Abdelsalam, M.G., Liégeois, J.P., Stern, R.J., 2002. The Saharan Metacraton. J. Afr. Earth Sci. 34, 109–117.
Acef, K., Liégeois, J.P., Ouabadi, A., Latouche, L., 2003. The Anfeg post-collisional Pan-African high-K calc-alkaline batholith (Central Hoggar, Algeria), result of the Latea microcontinent metacratonisation. J. Afr. Earth Sci. 37, 295–311.
Almond, D.C., 1980. Precambrian events at Sabaloka, near Khartoum, and their significance in the chronology of the basement of north-east Africa. Prec. Res. 13, 44–62.
André, L., Klerkx, J., Busrewil, M.T., 1991. Geochemical and Rb–Sr isotopic data on felsic rocks from the Jabal al Aiwaynat alcaline intrusive complex (SE Libya). In: Salem, M.J., Busrewil, M.T., Ben Ashour, A.M. (Eds.), The Geology of Libya, vol. 7. Elsevier, Amsterdam, pp. 2511–2527.
Avigad, D., Kolodner, K., McWilliams, M., Persing, H., Weissbrod, T., 2003. Origin of northern Gondwana Cambrian sandstone revealed by detrital zircon SHRIMP dating. Geology 31, 227–230.
Avigad, D., Stern, R.J., Beyth, M., Miller, N., McWilliams, M.O., 2007. Detrital zircon U–Pb geochronology of Cryogenian diamictites and Lower Paleozoic sandstone in Ethiopia (Tigrai) Age constraints on Neoproterozoic glaciation and crustal evolution of the southern Arabian–Nubian Shield. Prec. Res. 154, 88–106.
Bailo, T., Schandelmeier, H., Franz, G., Sun, C.-H., Stern, R.J., 2003. Plutonic and metamorphic rocks from the Keraf Suture (NE Sudan): a glimpse of Neoproterozoic tectonic evolution on the NE margin of W. Gondwana. Prec. Res. 123, 67–80.
Barth, H., Meinhold, K.D., 1979. Mineral Prospecting in the Bayuda Desert. Part I. Sudanese German Exploration Project, Technical Report, BGR, Hannover, 336 p.
Black, L.P., Kamo, S.L., 2003. TEMORA 1 a new zircon standard for U–Pb geochronology. Chem. Geol. 200, 155–170.
Bingen, B., Skår, Ø., Marker, M., Sigmond, E.M.O., Nordgulen, Ø., Ragnhildsveit, J., Mansfeld, J., Tucker, R.D., Liégeois, J.P., 2005. Timing of continental building in the Sveconorwegian orogen SW Scandinavia. Norwegian J. Geol. 85, 87–116.
Conticelli, S., Manetti, P., Capaldi, G., Poli, G., 1995. Petrology, mineralogy and isotopes in olivine mela-nephelinites, basanites and carbonatites from Uwaynat region, south east Libya: inferences on their genesis. Afr. Geosci. Rev. 2 (1995), 227–245.
Davidson, J.P., Wilson, I.R., 1989. Evolution of an alkali basalt–trachyte suite from Jebel Marra volcano, Sudan, through assimilation and fractional crystallization. Earth Planet. Sci. Lett. 95, 141–160.
De Wit, M.J., Bowring, S., Dudas, F., Kamga, G., 2005. The great Neoproterozoic central Saharan Arc and the amalgamation of the North African Shield. In: Abstr. Vol., Joint Annual GAC-MAC Meeting, Halifax, Canada.
Duchesne, J.C., Berza, I.T., Liégeois, J.P., Vander Auwera, J., 1998. Shoshonitic liquid line of descent from diorite to granite: the late Precambrian post-collisional Tismana pluton (South Carpathians, Romania). Lithos 45, 281–303.
Harris, N.B.W., Hawkesworth, C.J., Ries, A.C., 1984. Crustal evolution in north-east and East Africa from model Nd ages. Nature 309, 773–776.
Harms, U., Schandelmeier, H., Darbyshire, D.P.F., 1990. Pan-African reworked early/middle Proterozoic crust in NE Africa west of the Nile: Sr and Nd isotope evidence. J. Geol. Soc. Lond. 147, 859–872.
Harms, U., Darbyshire, D.P.F., Denkler, T., Hengst, M., Schandelmeier, H., 1994. Evolution of the Neoproterozoic Delgo suture zone and crustal growth in northern Sudan: geochemical and radiogenic isotope constraints. Geol. Rundsch. 83, 591–603.
Hart, S.R., 1984. A large-scale isotope anomaly in the southern hemisphere mantle. Nature 309, 753–757.
Klerkx, J., Deutsch, S., 1977. Résultats préliminaires obtenus par la méthode Rb/Sr sur l'âge des formations précambriennes de la région d'Uweinat (Libye). Musée Royal Afrique Centrale, Département Géologie Minéralogie Rapport Annuel 1976, pp. 83–94.
Kröner, A., Stern, R.J., Dawoud, A.S., Compston, W., Reischmann, T., 1987. The Pan-African continental margin in northeastern Africa: evidence from a geochronological study of granulites at Sabaloka, Sudan. Earth Planet. Sci. Lett. 85, 91–104.
Küster, D., 1995. Rb–Sr isotope systematics of muscovite from Pan-African granitic pegmatites of Western and Northeastern Africa. Mineral. Petrol. 55, 71–83.
Küster, D., Harms, U., 1998. Post-collisional potassic granitoids from the southern and northwestern parts of the Late Neoproterozoic East African Orogen: a review. Lithos 45, 177–195.
Küster, D., Liégeois, J.P., 2001. Sr, Nd isotopes and geochemistry of the Bayuda Desert high-grade metamorphic basement (Sudan): an early Pan-African oceanic convergent margin, not the edge of the East Saharan ghost craton? Prec. Res. 109, 1–23.
Liégeois, J.P., Navez, J., Hertogen, J., Black, R., 1998. Contrasting origin of post-collisional high-K calc-alkaline and shoshonitic versus alkaline and peralkaline granitoids. Lithos 45, 1–28.
Liégeois, J.P., Latouche, L., Boughara, M., Navez, J., Guiraud, M., 2003. The LATEA metacraton (Central Hoggar, Tuareg Shield, Algeria): behaviour of an old passive margin during the Pan-African orogeny. J. Afr. Earth Sci. 37, 161–190.
Ludwig, K.R., 2000. SQUID 1.00: a user's manual. Berkeley Geochronology Center Special Publication, vol. 2, pp. 1–19.
Ludwig, K.R., 2003. Isoplot 3.00, a geochronological toolkit for Microsoft Excel. Berkeley Geochronology Center Special Publication no. 4, 69 pp.
Lundmark, A.M., Corfu, F., 2008. Late-orogenic Sveconorwegian massif anorthosite in the Jotun Nappe Complex, SW Norway, and causes of repeated AMCG magmatism along the Baltoscandian margin. Contrib. Mineral. Petrol. 155, 147–163.
Maxson, J., Tikoff, B., 1996. Hit-and-run collision model for the Laramide orogeny, western United States. Geology 24, 968–972.
Meinhold, K.D., 1979. The Precambrian basement complex of the Bayuda Desert, northern Sudan. Rev. Géol. Dyn. Géogr. Phys. 21, 395–401.
Nelson, B.K., De Paolo, D.J., 1985. Rapid production of continental crust 17 to 1. 9 b. y. ago: Nd isotopic evidence from the basement of N. America mid-continent. Geol. Soc. Am. Bull. 96, 746–754.
Plumb, K.A., 1991. New Precambrian time scale. Episodes 14, 139–140.
Pudlo, D., Franz, G., 1994. Dike rock generation and magma interactions in the Bir Safsaf igneous complex, south-west Egypt: implications for the Pan-African evolution of NE Africa. Geol. Rundsch. 83, 523–536.
Pupin, J.P., 1980. Zircon and granite petrology. Contrib. Mineral. Petrol. 73, 207–220.
Ries, A.C., Shackelton, R.M., Dawoud, A.S., 1985. Geochronology, geochemistry and tectonics of the NE Bayuda Desert N Sudan: implication for the western margin of the late Proterozoic fold belt of NE Africa. Prec. Res. 30, 43–62.
Romer, R.L., Heinrich, W., Schröder-Smeibidl, B., Meixner, A., Fischer, C.-O., Schulz, C., 2005. Elemental dispersion and stable isotope fractionation during reactive fluid-flow and fluid immiscibility in the Bufa del Diente aureole, NE-Mexico: evidence from radiographies and Li, B, Sr, Nd, and Pb isotope systematics. Contrib. Mineral. Petrol. 149, 400–429.
Schandelmeier, H., Utke, A., Harms, U., Küster, D., 1990. A review of the Pan-African evolution of NE Africa: Towards a new dynamic concept for continental NE Africa. Berl. Geowiss. Abh. A120, 1–14.
Schandelmeier, H., Wipfler, E., Küster, D., Sultan, M., Becker, R., Stern, R.J., Abdelsalam, M.G., 1994a. Atmur-Delgo suture: a Neoproterozoic oceanic basin extending into the interior of northeast Africa. Geology 22, 563–566.
Schandelmeier, H., Abdel Rahman, E.M., Wipfler, E., Küster, D., Utke, A., Matheis, G., 1994b. Late Proterozoic magmatism in the Nakasib suture, Red Sea Hills, Sudan. J. Geol. Soc. Lond. 151, 485–497.
Stacey, J.S., Kramers, J.D., 1975. Approximation of terrestrial lead isotope evolution by a two-stage model. Earth Planet. Sci. Lett. 26, 207–221.
Stern, R.J., 1994. Neoproterozoic (900–550 Ma) arc assembly and continental collision in the East African Orogen: implications for the consolidation of Gondwanaland. Annu. Rev. Earth Planet. Sci. 22, 319–351.
Stern, R.J., 2008. Neoproterozoic crustal growth: the solid Earth system during a critical episode of Earth history. Gondwana Res., doi:10.1016/j.gr.2007.08.006 1276.
Stern, R.J., Dawoud, A.S., 1991. Late Precambrian (740 Ma) charnockite, enderbite, and granite from Jebel Moya, Sudan: a link between the Mozambique Belt and the Arabian-Nubian Shield? J. Geol. 99, 648–659.
Stern, R.J., Kröner, A., 1993. Geochronologic and isotopic constraints on Late Precambrian crustal evolution in NE Sudan. J. Geol. 101, 555–574.
Stern, R.J., Abdelsalam, M.G., 1998. Formation of Juvenile Continental Crust in the Arabian–Nubian Shield: evidence from Granitic rocks of the Nakasib Suture, NE Sudan. Geol. Rundsch. 87, 150–160.
Stoeser, D.B., Frost, C.D., 2006. Nd, Pb, Sr, and O isotopic characterization of Saudi Arabian Shield terranes. Chem. Geol. 226, 163–188.
Vail, J.R., 1971. Geological reconnaissance in part of Berber District, Northern Province. Geological Survey Department of the Sudan, Bulletin 18, Khartoum, 76 pp.
Vail, J.R., 1976. Outline of the geochronology and tectonic units of the basement complex of Northeast Africa. Proc. Royal Soc. London, Ser. A 350, 127–141.
Vail, J.R., 1988. Tectonics and evolution of the Proterozoic basement of Northeastern Africa. In: El-Gaby, S., Greiling, R. (Eds.), The Pan-African Belt of Northeast Africa and Adjacent Areas. Vieweg und Sohn, Braunschweig, pp. 195–226.
Vail, J.R., 1989. Whither the Kibaran in NE Africa. IGCP Newsletter 255, Bull. 2, pp. 93–97.

Wiedenbeck, M., Allé, P., Corfu, F., Griffin, W.L., Meier, M., Oberli, F., Von Quadt, A., Roddick, J.C., Spiegel, W., 1995. Three natural zircon standards for U–Th–Pb, Lu–Hf, trace element and REE analyses. Geostandards Newslett. 19, 1–23.

Williams, I.S., 1998. U–Th–Pb geochronology by ion microprobe. In: McKibben, M.A., Shanks, W.C., III, Ridley, W.I. (Eds.), Applications of Microanalytical Techniques to Understanding Mineralizing Processes. Rev. Econ. Geol. 7, pp. 1–35.

Williams, I.S., Buick, I.S., Cartwright, I., 1996. An extended episode of early Mesoproterozoic metamorphic fluid flow in the Reynold Range, central Australia. J. Metamorph. Geol. 14, 29–47.

Zimmer, M., Kröner, A., Jochum, K.P., Reischmann, T., Todt, W., 1995. The Gabal Gerf complex: a Precambrian N-MORB ophiolite in the Nubian Shield NE Africa. Chem. Geol. 123, 29–51.